Doris Martina Grössl, BSc

Functionalization of Group 14 Metal *meso*-Tetraphenylporphyrins

Master's Thesis

to achieve the university degree of

Diplom-Ingenieurin

Master's degree program: Technical Chemistry

submitted to

Graz University of Technology

Supervisor

Univ.-Prof. Dipl.-Chem. Dr.rer.nat. Frank Uhlig

Institute of Inorganic Chemistry

Graz, March 2020

Affidavit

I declare that I have authored this thesis independently, that I have not used other than the declared sources/resources, and that I have explicitly indicated all material which has been quoted either literally or by content from the sources used. The text document uploaded to TUGRAZonline is identical to the present master's thesis.

Datum/ Date	Unterschrift/ Signature

Für meine Eltern

"Wanting to be someone else is a waste of who you are "

- *Kurt Cobain*

Danksagung

An dieser Stelle möchte ich mich ausdrücklichst bei Frank Uhlig für die Möglichkeit meine Masterarbeit in seiner Arbeitsgruppe zu verfassen bedanken. Vielen Dank für die Motivation, das Vertrauen und die Ratschläge.

Ein besonderer Dank gilt Stefan Stadlbauer, der mich seit meiner Bachelorarbeit nicht mehr los geworden ist. Danke, dass du mir deine Begeisterung für Porphyrine und die Forschung im Allgemeinen weitergegeben hast, für das Wissen, die interessanten Gespräche und die Geduld, die du mir gegenüber aufgebracht hast.

Ich möchte mich auch herzlichst bei Yaiza, Moni, Babsi und Marit bedanken, die dieses Institut am Laufen halten.

Weiterer Dank gilt Philipp Frühwirth für die EPR Messungen und Beantwortung all meiner lästigen Fragen zu diesem Thema.

Außerdem möchte ich mich bei all meinen Kollegen am Institut für die Tipps, lustigen Mittagspausen und die Unterstützung bedanken.

Besonders dankbar bin ich allen Mitgliedern der „Labor Lamas" bzw. „Partnerbörse": Yaiza, Philipp, Philipp, Feri, Christoph und Benjamin. Danke für die zahlreichen Therapiesitzungen und für die lustige Zeit.

Einen weiteren besonderen Dank gilt Johannes für die großartige emotionale Unterstützung und das offene Ohr für all meine Jammereien. Thank you for always picking me up from the floor.

Ich möchte mich auch bei all meinen Freunden und Studienkollegen, insbesondere bei Sabi, Philipp, Johanna, Eva, Snjezi, Rene und Alina für die Motivation und die lustige Studienzeit bedanken.

Weiterhin möchte ich bei meiner Schwester Jasmin bedanken. Danke für die Freundschaft und die Inspiration durch deine Kreativität.

Abschließend bedanke ich mich bei meinen Eltern, die immer an mich glauben und für die finanzielle Unterstützung, ohne welche mein Studium nicht möglich gewesen wäre.

Abstract

Porphyrins bearing a group 14 metal like Si, Ge or Sn as a center atom are very well known in literature. Applications span from opto-electronic devices (e.g. solar cells) to medical applications (e.g. photodynamic therapy). Recently the research focuses is on the synthesis and characterization of new axial ligands to these otherwise well-known systems. This thesis deals with the synthesis of group 14 *meso*-tetraphenylporphyrins bearing hydrides as axial ligands. Hydrides as axial ligands to porphyrins are the first showing s hybridization character. They were subsequently characterized via NMR, UV/VIS, ATR-FTIR and EPR.

Kurzfassung

Porphyrine mit einem Gruppe 14 Metall wie Si, Ge oder Sn als Zentralatom sind sehr bekannt in der Literatur. Anwendungsgebiete dieser Systeme spannen von optisch-elektronischen Geräten (z.B. Solarzellen) bis zu medizinischen Anwendungen (wie z.B. Photodynamische Therapie). In letzter Zeit befasst sich der Forschungsschwerpunkt mit der Synthese und Charakterisierung von neuen axialen Liganden zu diesen anderenfalls sehr bekannten Systemen. Diese Masterarbeit behandelte die Synthese von Gruppe 14 *meso*-Tetraphenylporphyrinen mit Hydriden als axiale Liganden. Hydride als axiale Liganden sind die ersten, welche einen s Hybridisierungscharakter aufweisen. Die synthetisierten Verbindungen wurde mittels NMR, UV/VIS, ATR-FTIR und EPR charakterisiert.

1 Table of Contents

Abbreviations

Por	Porphyrin
NMR	Nuclear Magnetic Resonance
EPR	Electron Paramagnetic Resonance
Et	Ethyl
Bu	Butyl
HOMO	Highest Occupied Molecular Orbital
LUMO	Lowest Unoccupied Molecular Orbital
TPP	*Meso*-Tetraphenylporphyrin
H$_2$TPP	Free Base *meso*-Tetraphenylporphyrin
OEP	Octaethylporphyrin
DIBAL	Diisobutylaluminiumhydride
THF	Tetrahydrofuran
FWHM	Full Width at Half Maximum
COSY	Correlation Spectroscopy
o-	*Ortho*
m-	*Meta*
p-	*Para*
i-	*Iso*
Tol	Toluene
T	Temperature
RT	Room Temperature
s	Singlet
brs	Broad Singlet
d	Doublet
tr	Triplet
hept	Heptett

eq	Equivalence
VT	Variable Temperature
Rel Int.	Relative Intensity
HMDS	Hexamethyldisilazane
n-**BuLi**	*n*-Butyllithium
DCM	Dichloromethane

2   Theoretical Background

2.1   General

Porphyrins are a highly conjugated class of macrocycles consisting of 4 pyrroles bridged via methine. Alterations in number of heteroatoms, substitution pattern and degree of conjugation gives a variety of derivatives as seen in Figure 1. [1]

Porphyrin   **Chlorin**   **Bacteriochlorin**

Figure 1 Core structures of porphyrin and other tetrapyrrolic derivatives [1]

Porphyrins play a vital role in many biological functions like in cytochromes as part of the electron transfer across the membranes of bacteria and mitochondria [2], as chlorophyll in the photosystem II for photosynthesis [3] and as part of the active site in oxygen-carrying hemoproteins [4]. Due to their vast importance it is therefore unsurprising that the first example of porphyrins was already described in 1900 by Nencki and Zeleski as part of the heme-complex. [1,5]

2.2   Applications

The photocatalytic activity of porphyrins and related systems make them suitable for widespread applications in environmental technology and medicine. In medicine porphyrins are for example used for the treatment of cancer cells in photodynamic therapy or as photoactive chemicals for antimicrobial textiles. [6,7] In both examples porphyrins act as a photosensitizer and rely on the formation of singlet oxygen ($^1O_2$) through type II photochemical reaction, there ground state molecules are excited to the singlet excited state by absorption of photons, transfer through

intersystem crossing into triplet excited states, which are then quenched by ground state oxygen ($^3O_2$) and yield singlet oxygen ($^1O_2$). [7] The generated singlet oxygen can subsequently inactivate gram-positive bacteria or destroy the cell tissue of cancer cells. [6,7]

In environmental applications Sn^{IV}porphyrins are placed onto silica nanoparticles, where the generated reactive singlet oxygen ($^1O_2$) degrades organic pollutants. [8]

In more recent publications porphyrins are described as possible materials for the application in solar cells. Porphyrins have been implemented in dye sensitized solar cells as well as bulk heterojunction solar cells as donor material which yield power conversion efficiencies up to 13%. [9–12] In these applications mostly Zn(II) and Mg(II) are used as central atoms as depicted by two examples in Figure 2. To expand the π-conjugated system the acidic meso position of the porphyrin ring has to be substituted.
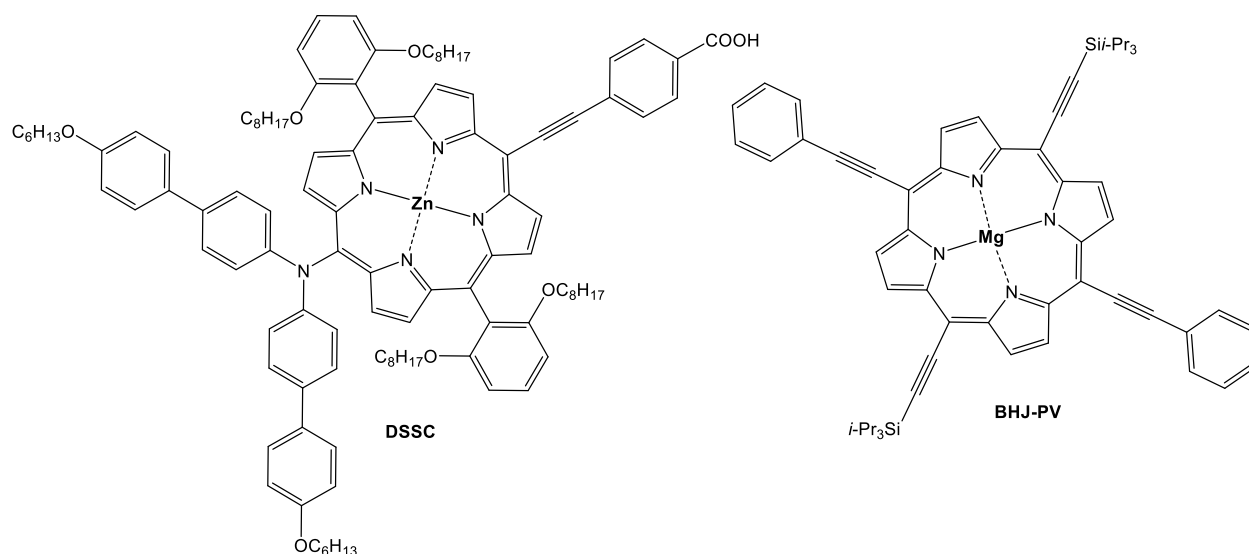
Figure 2 Examples of a porphyrin used in a DSSC (left) [11] and BHJ-PV (right) [9]

Several patents are describing the use of a wide variety of other metals in different oxidation states in combination with various (poly)porphyrins. [12–14] However, it is on one hand doubtful that all the metals in oxidation state II mentioned in patents [14,13] were really tested and on the other hand the required "fused polycyclic and fused heterocyclic aromatic" substituents on the porphyrin skeleton does not simplify synthesis. Examples are illustrated in Figure 3. [14]
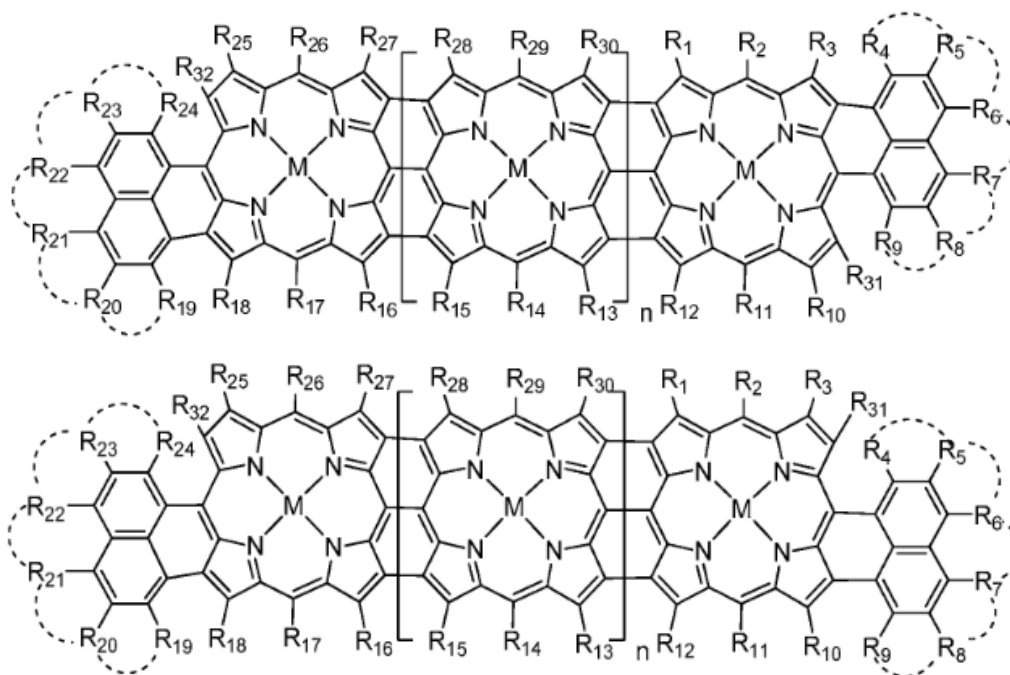
Figure 3 Examples of (poly)porphyrinskeletons of patent [14]; preferably M= Zn, Pb, Sn, ClAl, SnO, $SnCl_2$, Pb(OAc) and $Sn(OH)_2$

Implementing group 14 metals of the oxidation state IV as the center atom carrying at least one organic, alkoxy or hydroxy substituent opens up the 3rd dimension through axial ligands as accomplished in previous work of our group. [15,16] C-bound Sn(IV) porphyrins are rare but have already described in literature. [17] The focus of previous publications is however only on the applicability as potential photodynamic therapeutic tools in medicine. New research describes porphyrins as seen in Figure 4 bearing Si^{IV}, Ge^{IV} or Sn^{IV} as probably suitable for acceptor application towards P3HT in thin film organic solar cells. [18]

E = Si, Ge, Sn
R = phenyl, pentyl or 9-phenanthryl
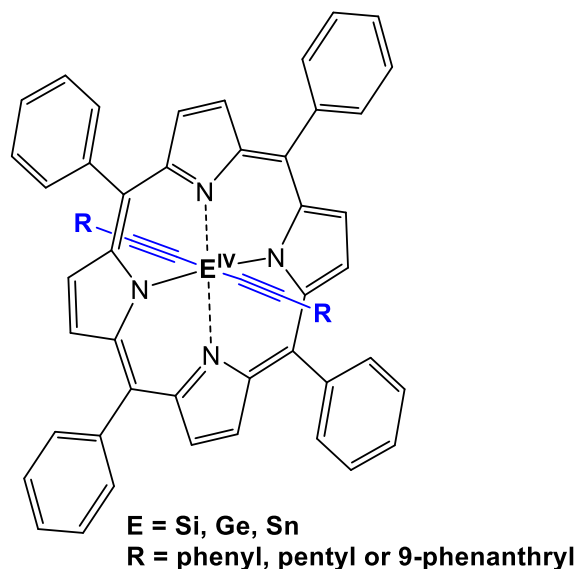
Figure 4 Porphyrin structure bearing E^{IV} (E=Si, Ge, Sn) as probable acceptor material for thin film organic solar cells [18]

2.3 Group 14 Porphyrin Complexes

Porphyrin complexes of the chemical formula $M(Por)X_2$ (Por= Porphyrin) for M=Ge and M=Sn have been known for a long time. Silicon porphyrins however only to a lesser extent due to its very high hydrolytic reactivity of $Si(Por)Cl_2$. The earliest report of organogermanium porphyrins as potential NMR shift reagents was published in 1973.

A wide range of Group 14 porphyrin complexes are reported to date. In general, the center metals are six-fold coordinated with trans axial ligands (except for two complexes which exhibit cis conformation) with the formula $M(Por)R_2$ and $M(Por)RX$ with X as a halogen. In general, five different synthetic routes to modify or implement axial ligands to those complexes have been described:

    I.   Reaction of $M(Por)X_2$ or $M(Por)OH_2$ with RLi or RMgBr [19]

    II.   Oxidative addition of RX to $M^{II}(Por)$ [19]

    III.   Metalation of $Li_2(Por)$ with R_2MX_2 [19]

    IV.   Photochemical cleavage of one R in $M(Por)R_2$ to form $M(Por)RX$ [19]

    V.   Redistribution reaction of $M(Por)R_1$ and $M(Por)X_2$ to form $M(Por)RX$ [16]

The five different synthetic routes to modify or implement axial ligands are illustrated in Figure 5.
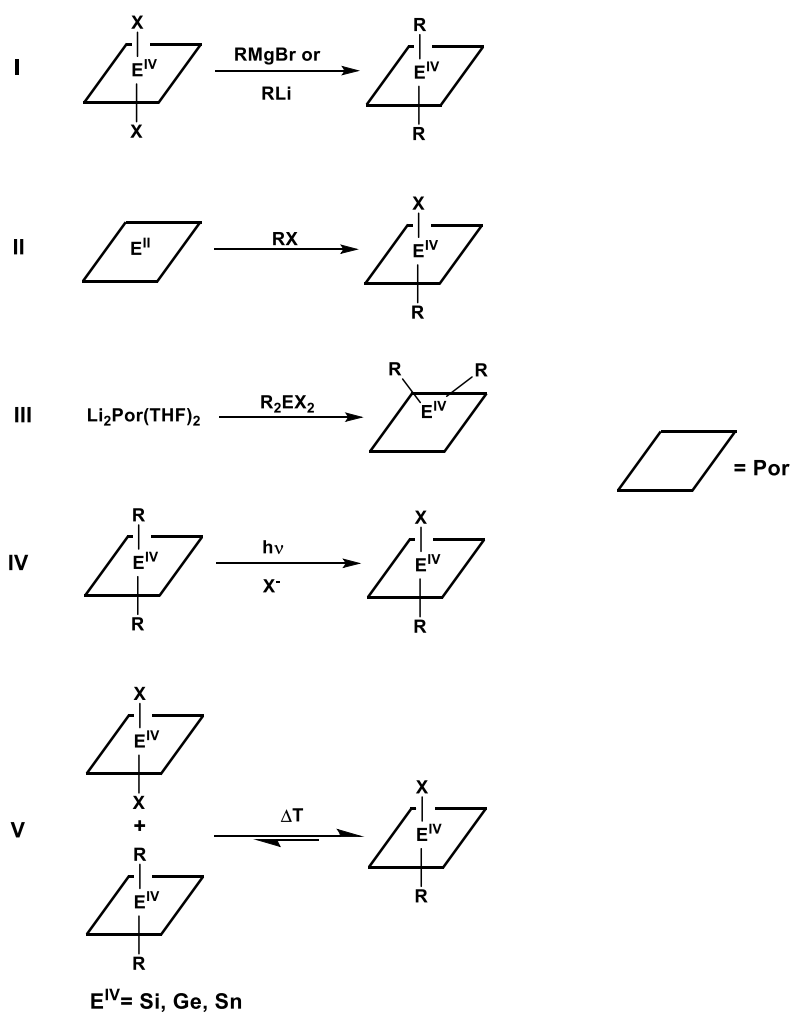
Figure 5 Synthetic routes for the preparation of M(Por)R$_2$ and M(Por)RX

These complexes show interesting properties. Si^{IV} porphyrins undergo homolytic cleavage of the axial Si-C bond under irradiation to form highly stable silicon diradicals at the groundstate, these diradicals can react with nitroxy compounds upon irradiation with visible light. Homolytic cleavage of the Si-O bond of the resulting dinitroxysilicon prophyrins through irradiation with visible light gives free radicals. This results in the possibility of using these silicon diradical as "photoswitchable radicals". [20] Ge^{IV} porphyrins can be used as chemical shift reagents due to their macrocyclic ring current as described by J. E. Maskasky and M. E. Kenney. [21] Dialkyl substituted germanium porphyrins also show interesting reactivities towards O$_2$ and light

producing organic peroxides. [22] Electrochemical investigations of R$_2$GeTPP even showed the synthesis of RXGeTPP by electrochemical oxidation. [23]

2.4 Stability

The stabilities with respect to demetallation vary dramatically, depending on size, oxidation state and degree of covalent bonding. Reduction of the oxidation state of a metal ion increases the size causing the complex to destabilize which results in demetallation. Some metalloporphyrin's also undergo photolytic degradation. [24] Group 14 porphyrin complexes are an interesting example regarding their high sensitivity to O$_2$, H$_2$O and light. [25,17] Diaryl compounds as axial ligands undergo cleavage of the M-C bond upon irradiation (provided under absence of O$_2$). The less stable dialkyl compounds even undergo decomposition upon irradiation. Tin examples show that the M-C lability is related to the p-character of the bond. Therefore the more electron-withdrawing alkynyl ligands are less reactive and can even be exposed to air in solid state for short periods of time. [18,19] Figure 6 shows examples of the different hybridization degrees (sp^3 [25], sp^2 [26] and sp [15]) of the C-atom bound to the Sn. Hydrogen atoms as axial ligands, which exhibit s character are to the best of our knowledge not known so far.
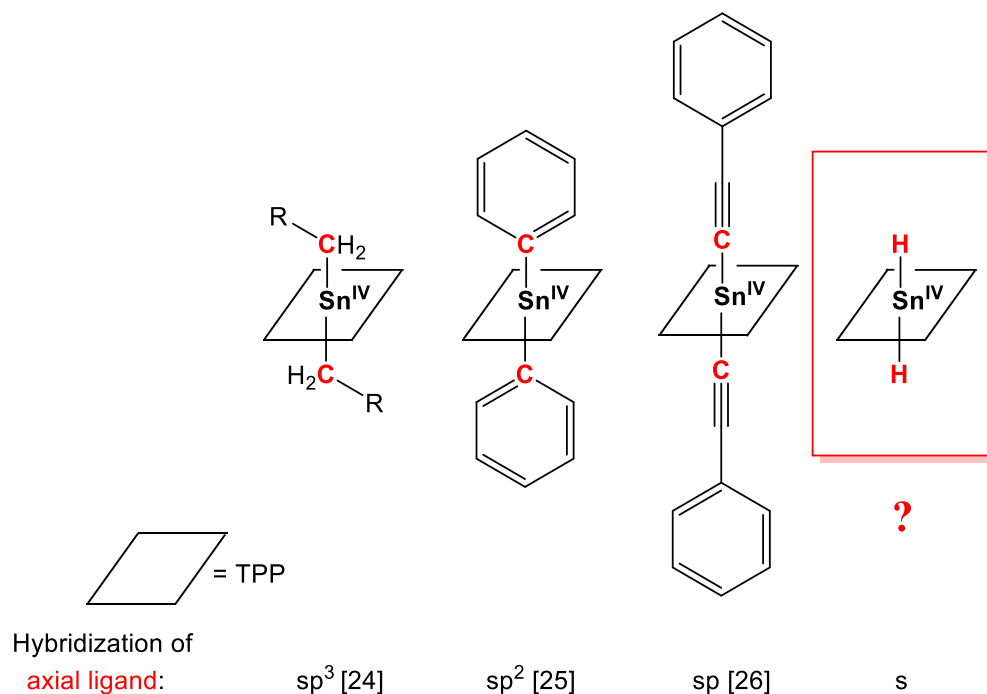
Figure 6 Sn^{IV}porphyrin species showing different hybridization of the axial ligand

2.5 Group 14 Hydrides

As mentioned in chapter 2.4, to the best of our knowledge, group 14 porphyrins with axial ligands exhibiting s character are not known which includes Group 14 porphyrin hydrides.

Metal hydrides are usually prepared by reducing the corresponding chlorides with $LiAlH_4$. [27] Other reduction reagents are R_2AlH, $NaBH_4$, $NaBH_3CN$, B_2H_6, LiH, $(MeSiHO)_n$, Et_3SiH, R_3SnH and $K(BEt_3)H$. [28,29]

The reactivity of organometallic hydrides $R_{4-n}MH_n$ in accordance with the dissociation energy of M-H bonds increases sharply as the atomic number of M increases. The thermal stability of these compounds decreases in the same direction. [30]

It is therefore unsurprising that only one six-fold coordinated tin hydride is published in literature (as displayed in Figure 7). [27] However further experimental information was not described. For completion two other complexes have to be mentioned, these however include the transition metals Fe and Ru. [31,32]

Concerning six-fold coordinated germanium hydrides there appear to be no examples published. Six-fold coordinated silicon hydrides are however commonly found in literature. Two examples are displayed in Figure 7. This fits the trend concerning the reactivity and dissociation energy of Group 14 M-H bonds. [33–37,27]
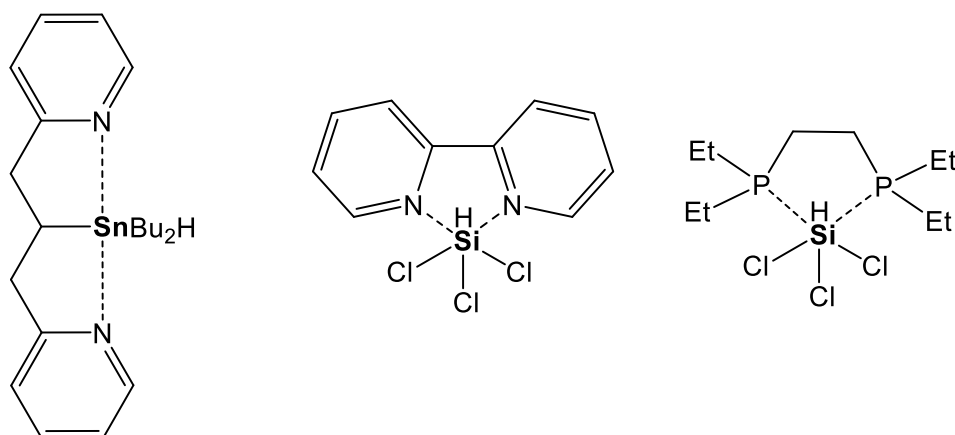
Figure 7 Examples for six-fold coordinated tin and silicon hydrides [27,36,35]

3 Results and Discussion

3.1 Characterization of Axially Substituted Group 14 Porphyrins

3.1.1 Characterization via NMR Spectroscopy [38]

The NMR spectra of porphyrins give certain chemical shifts of unusual magnitude. [39] NMR active nuclei of axial ligands and in proximity to the porphyrin centre are usually high field shifted while NMR active nuclei on the periphery of the porphyrin ring are low field shifted. [38] These effects are attributable to the "ring current" formed by the π electrons of the porphyrin ring and can be explained via the differential Biot-Sarvat law. [39,40] An external magnetic field (B_{ext}) induces a diamagnetic ring current, which causes a magnetic field (B'). This magnetic field B' counteracts B_{ext} according to Lenz's rule. Therefore, the two magnetic fields on the exterior ring current are aligned and point in the same direction causing the equatorial NMR active nuclei of the porphyrin ring to be low field shifted. NMR active nuclei of the axial ligands on the other hand are high field shifted due to the opposing direction of B' and B_{ext}. [38] The behaviour of these magnetic fields was documented for $(HO)_2SnTPP$ in [41], demonstrated by Stadlbauer in this master thesis [38] as shown in Figure 8 and can be described mathematically through Equation 1, Equation 2 and Equation 3. The amount of porphyrins present in one sample can best be determined via the shifts of the β-hydrogen atoms, which are typically in the range of +8.8 ppm to +9.4 ppm for *meso*-tetraphenyl porphyrins in $CDCl_3$. [17,42] Protons of axial ligands can be assigned easily as a result of the negative chemical shift due to the counteracting magnetic field, especially protons closest to the porphyrin center. [38] A correlation between the polar distance (R), defined as the distance between the metal center of the macrocycle to the hydrogen atom of interest (as depicted by Figure 9), and incremental chemical shift ($\Delta\delta$), which is the difference between the ^{1}H-NMR shift of the free ligand and the corresponding ^{1}H-NMR shifts of the ligand in axial position of the macrocycle, was first described for phthalocyanines theoretically [43] and expanded to *meso*-tetraphenyl porphyrins [18].
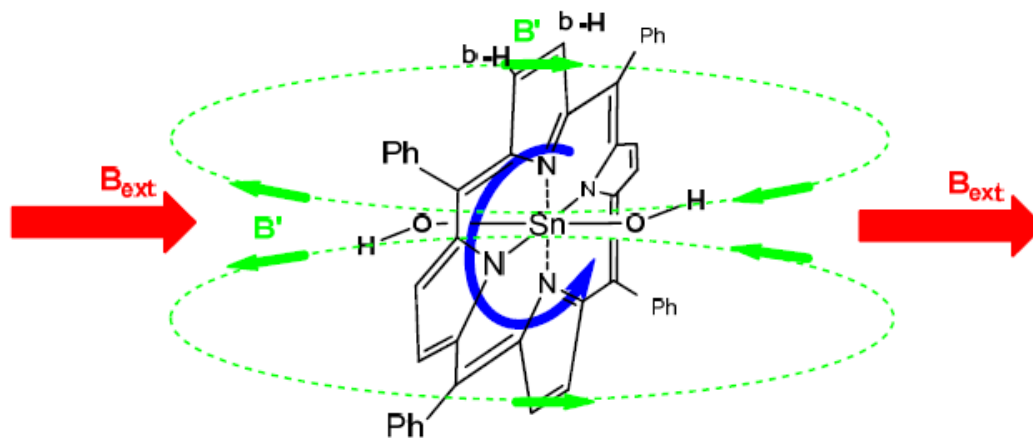
Figure 8 Influence of the π-ring current demonstrated on (HO)₂SnTPP (with permission of [38])

$$\overrightarrow{B_{loc}} = \overrightarrow{B_{ext}} + \overrightarrow{B'}$$

Equation 1 Magnetic flux density

$$B_{loc\,eq} > B_{loc\,axial}$$

$$w = \gamma * B_{loc}$$

Equation 2 Resonance frequency

$$w_{eq} > w_{axial}$$

$$\delta = \frac{10^6(w - w_{St})}{w_{St}}$$

Equation 3 Chemical shift

$$\delta_{eq} > \delta_{axial}$$

B .... Magnetic flux density [T]

γ .... Gyromagnetic constant [$s^{-1}T^{-1}$]

w .... Resonance frequency [s^{-1}]

w_{St} .... Resonance frequency of the standard [s^{-1}]

δ .... Chemical shift [ppm] [38]
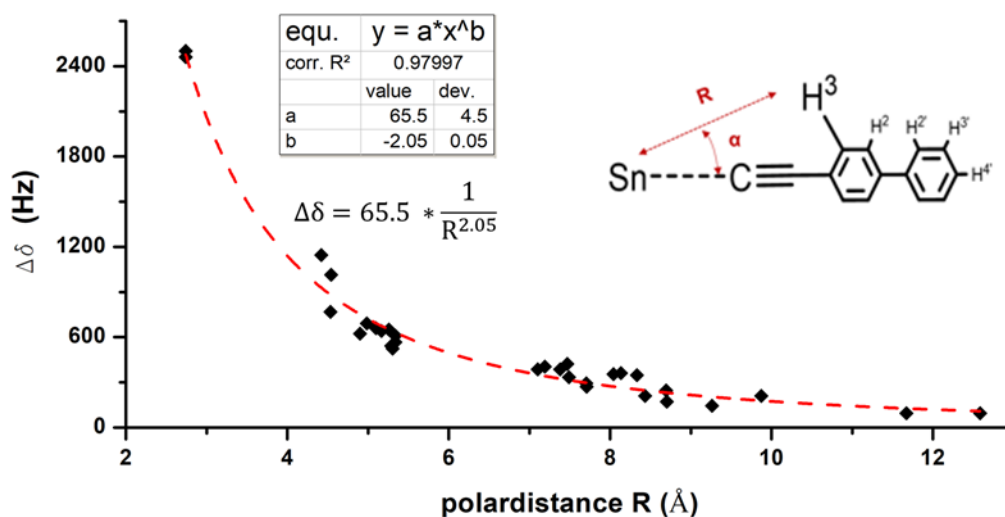
Figure 9 Relation of incremental chemical shift (Δδ) vs polar distance (R) at 300 K in C_6D_6 (with permission of [18])

Figure 9 describes this relation through a power law, making it a convenient tool in the determination of the approximate shifts of axial ligands and therefore identification through ^{1}H-NMR spectroscopy.

3.1.2 Characterization via UV/VIS Spectroscopy

The information summarized in this chapter is assorted from [38,44,45].

Porphyrins obtain characteristic UV/VIS spectra with high intensities attributed to π-π* transitions. Gouterman described in the 1980s the four-orbital model for interpreting UV/VIS spectra of porphyrins and related systems. It considers excited states from transitions between HOMO and HOMO-1 π-orbitals and LUMO and LUMO+1 π* orbitals. For porphyrins with a 4-fold symmetry (D_{4h}), the LUMO and LUMO-1 orbitals (e_{gx} and e_{gy}) are degenerate and the HOMO and HOMO-1 orbitals (a_{2u} and a_{1u}) are nearly degenerate as demonstrated in Figure 12. The excited states originating from the transitions a_{1u}->e_{gy} and a_{2u}-> e_{gx} are x-polarized while excited states from a_{1u}->e_{gx} and a_{2u}-> e_{gy} transitions are y-polarized. These excited states are split in energy due to configuration interaction into two pairs of degenerate ^1E_u low-energy and low intensity transitions, called Q-band (Q_x and Q_y) and two high energy and high intensity transitions, called Soret band (B_x and B_y). Besides the Q- and Soret band there is also a third band, called N-band,

which is the transition from the singlet ground state to the third excited singlet state and located in the UV region. Metal-free porphyrins inhibit D_{2h} symmetry, where the LUMO and LUMO+1 orbitals are not degenerated, resulting in further splitting of the Q_x, Q_y and B_x, B_y transitions.
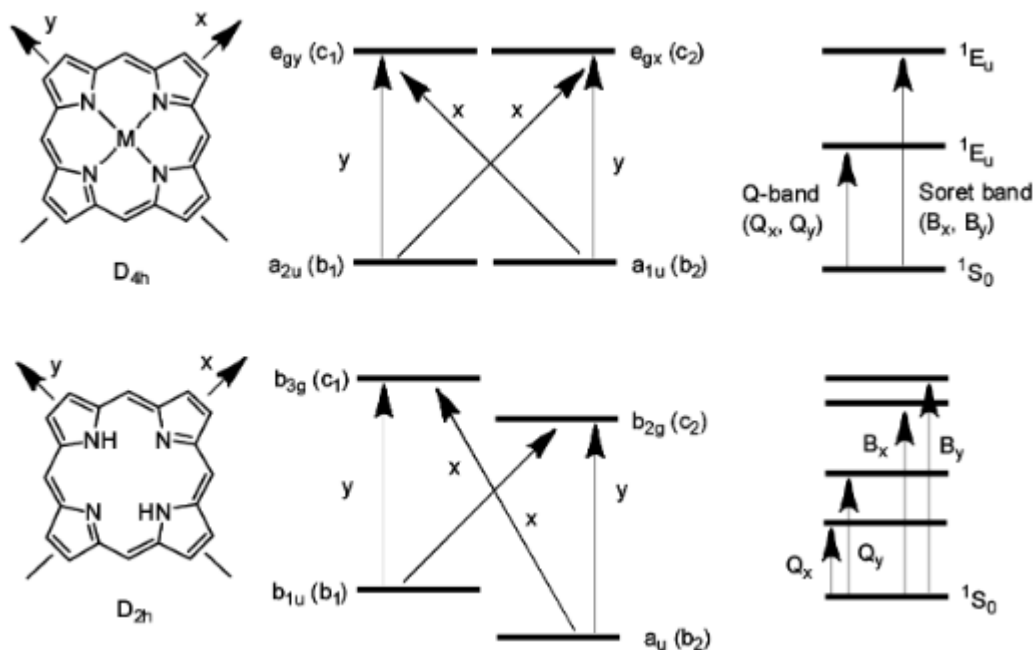
Figure 10 Gouterman's four- orbital model for porphyrins with D_{4h} and D_{2h} symmetry (by [44])

Axial ligands, which affect the excited states provoke a shift of certain bands in the UV/VIS spectra. It was observed that more electropositive ligands decrease the absorption energies which results in a bathochromic shift. UV/VIS spectroscopy can therefore be used as an additional characterization tool for the identification of porphyrin species. [15]

In contrast to Sn(IV) porphyrins with D_{4h} symmetry, Sn(II) porphyrins exhibit a "hyper-type" spectrum. An additional bathochromic absorption occurs in cause of charge-transfer transitions $a_{2u} \rightarrow e_g$ from the tin to the macrocycle through the free electron pair of the tin(II) atom. [46] Figure 11 illustrates examples of UV/VIS spectra of D_{4h} (Cl_2SnTPP, purple) and D_{2h} (H_2TPP, blue) symmetry and also the "hyper-type" spectrum of Sn(II)TPP (green). The already literature known UV/VIS spectra [38,17] shown below were measured independently.
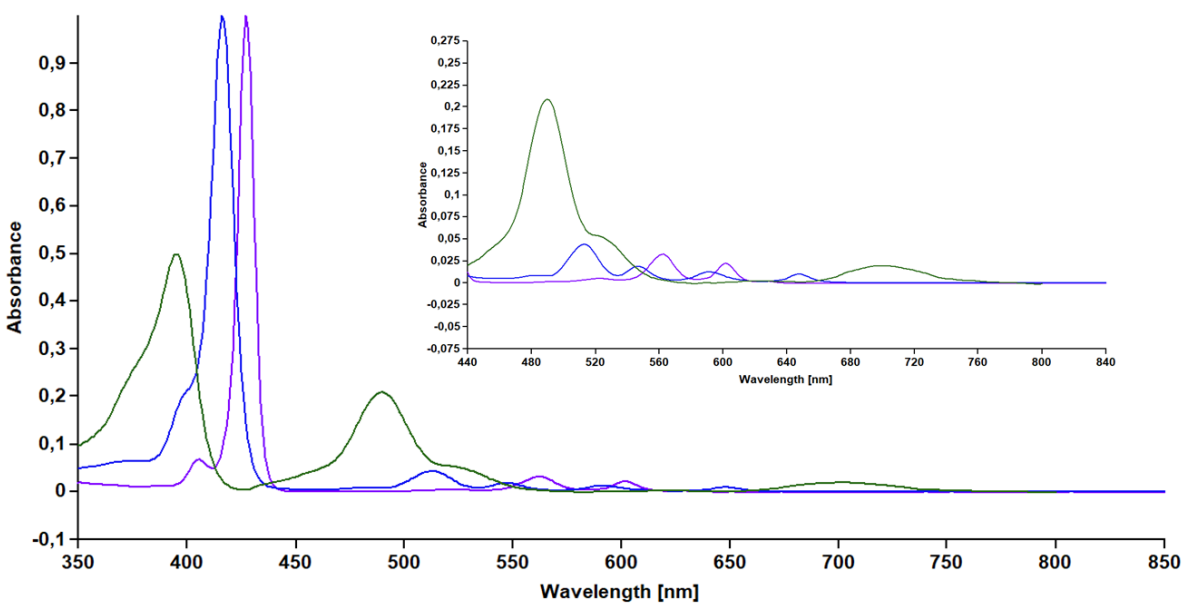
Figure 11 UV/VIS spectra of H_2TPP (blue), Cl_2SnTPP (purple) and Sn(II)TPP (green)

3.1.3 Characterization via EPR Spectroscopy

Electron Paramagnetic Resonance (EPR) Spectroscopy is a characterization method for the investigation of substances with unpaired electronic spins (as free radicals, transition-metal compounds and biradicals). EPR is complementary to NMR spectroscopy, as resonances for paramagnetic substances in NMR are typically broadened by tens of hertz. The principle of EPR spectroscopy is the Zeeman effect, which states that in the presence of a magnetic field (B_0), the magnetic moment of a spin ½ exhibit two orientations in the field. Therefore, a molecule or ion holding one unpaired electron has two electron-spin energy levels, with the energy difference described by Equation 4: [47]

$$\Delta E = g\mu_B B_0$$

Equation 4 Zeeman-Effect

ΔE .... Energy Difference [J]

g .... G-Factor ("Landé Factor")

μ_B .... Bohr Magneton [J/T]

B_0 .... Magnetic Field Strength [T]

An electromagnetic wave of certain frequency is able to excite the electronic spin from its low energetic lever to its high one. In ESR spectroscopy a fixed excitation frequency and a sweeping magnetic field are applied and the relation expressed as:

$$h\nu = g\mu_B B_0$$

The g value of organic free radicals is close to that of a free electron, for porphyrin radicals it typically ranges between 1.999 and 2.006. [48]

If the electron can interact with the nuclear magnetic dipole of neighboring atoms hyperfine coupling occurs, by which structural assumptions can be made. [47]

ESR studies of porphyrin radicals include the chemical properties and electronic structure of reduced and oxidized porphyrins. Radicals can be generated chemically, photo chemically and electrochemically. Electrons can be added and subtracted to the porphyrin ring to yield either radical anions or radical cations. [49]

3.2 Attempted Synthesis of H₂SnTPP

Starting from the educt Cl₂SnTPP, which was synthesized according to [15], the synthesis of the literature unknown compound H₂SnTPP was attempted by reduction with NaH, H₃B*THF, K[BEt₃]H, DIBAL and LiAlH₄. The reduction attempts with NaH and BH₃ lead to no reaction even under reflux heating. Reactions of Cl₂SnTPP with K[BEt₃]H, DIBAL and LiAlH₄ at -40 °C, as demonstrated in Scheme 1 did not yield the desired H₂SnTPP, however resulted in the reduction of Sn(IV) to Sn(II)TPP as confirmed by ¹H-NMR and UV/VIS.
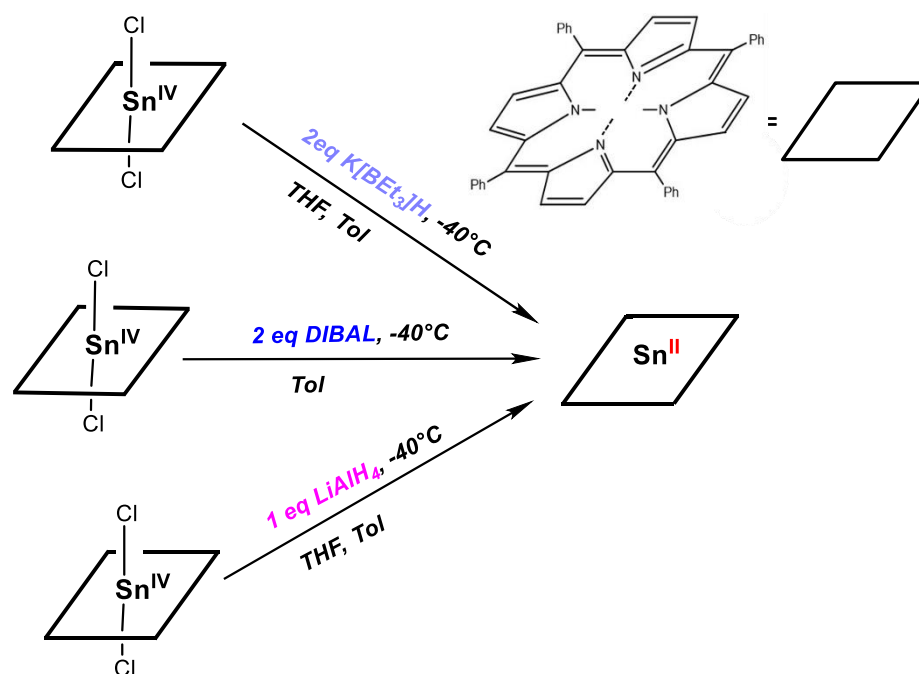
Scheme 1 Reduction of Cl₂SnTPP to Sn(II)TPP

Although the desired product was not obtained, the reactions described in Scheme 1 show new synthetic routes towards Sn(II)TPP. So far three ways to obtain the compound are known in literature as described in Scheme 2. [50,38]

Scheme reactions:

$$\text{H}_2\text{TPP} + Sn\text{Cl}_2 \xrightarrow{\text{THF, pyridine (115°C)}} \text{Sn}^{II}\text{TPP}$$

$$2\ \text{[Naphthalene]}^{\bullet -}\text{Na}^+ + \text{Cl}_2\text{Sn}^{IV}\text{TPP} \xrightarrow[\text{-2 Naphtalene}]{C_6H_6,\ \text{-2 NaCl}} \text{Sn}^{II}\text{TPP}$$

$$2/x\ (Ph_3Sn)_xM + \text{Cl}_2\text{Sn}^{IV}\text{TPP} \xrightarrow[{-^{(y-2)}/_x\ (Ph_3Sn)_xM}]{Tol,\ T,\ -^2/_x\ MCl_x} \text{Sn}^{II}\text{TPP}$$

M= Na, K, Li, Mg
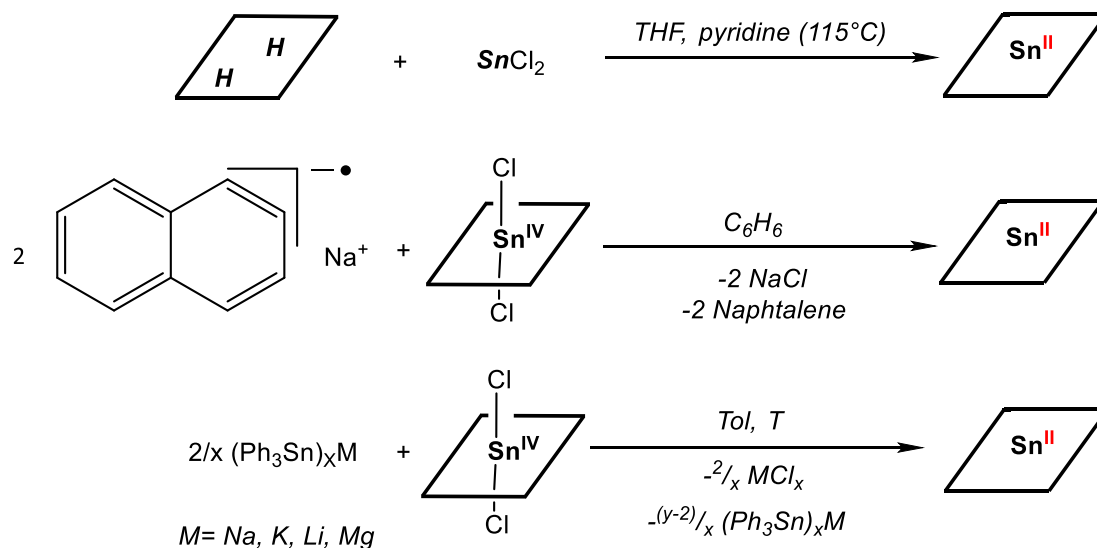
Scheme 2 Literature known reactions yielding Sn(II)TPP

3.2.1 Variable Temperature ^{1}H-NMR Study

To investigate the reaction mechanism and possible intermediates leading to the formation of Sn(II)TPP (Scheme 1) a variable temperature (VT) ^{1}H-NMR study of the reduction with LiAlH$_4$ was conducted. A color change from purple (educt) to red and then green (Sn(II)TPP) can be observed. Figure 12 lays out the ^{1}H-VT-NMR of the red colored intermediate in THF-d$_8$ at -40 °C (2), -20 °C (3), 0 °C (4) and 22 °C (5). Furthermore the ^{1}H-NMR spectra of Cl$_2$SnTPP in THF-d$_8$ is displayed for comparison.
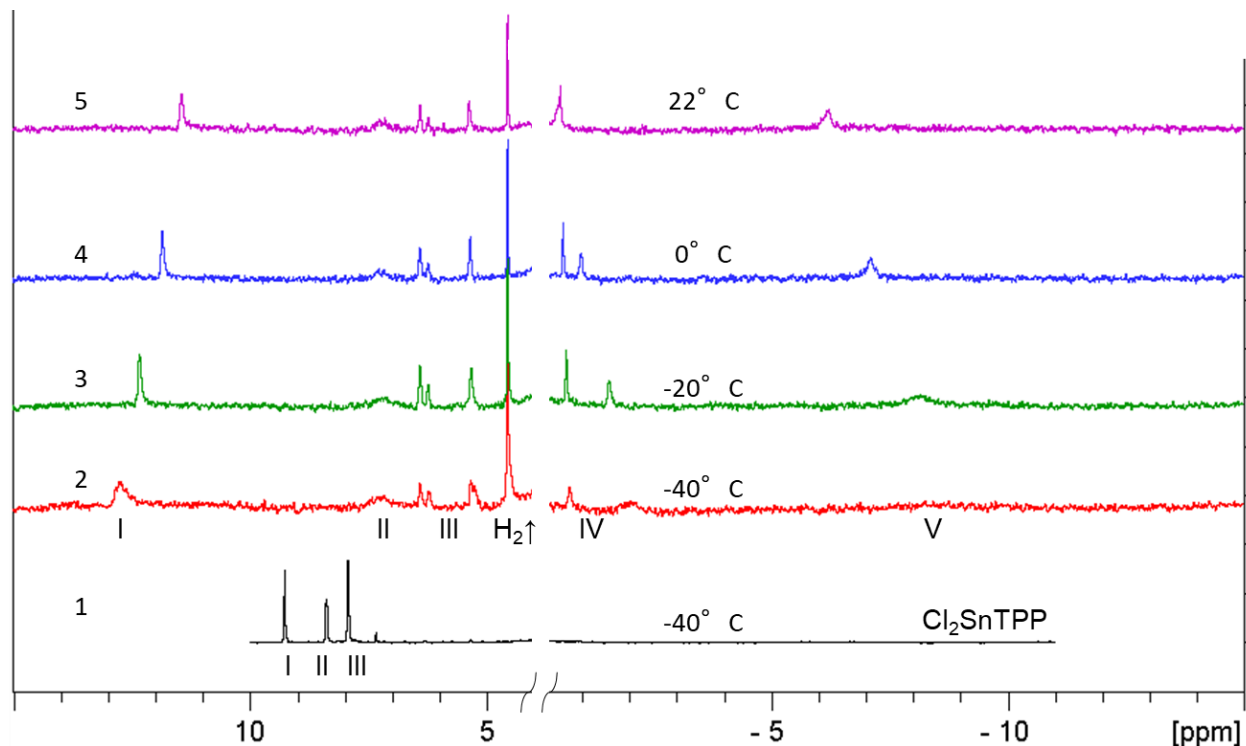
Figure 12 VT-^{1}H-NMR of Cl$_2$SnTPP (1) at -40 °C and the reaction mixture in THF-d$_8$ at -40 °C – 22 °C (2-5)

The chemical shifts and their full width at half maximum (FWHM) of the ^{1}H-NMR spectra of Figure 12 are listed in Table 1. FWHM values up to 178 Hz were obtained. This severe line broadening and the T-dependency of shifts I, IV and V indicate the formation of a paramagnetic substance. Kadish et al. also observed broad resonances in the ^{1}H-NMR of (C$_6$H$_5$)$_2$GeTPP and (C$_6$H$_5$CH$_2$)$_2$GeTPP in THF-d$_8$ after photolysis which were proven to arise from a π radical anion. [51]

Table 1 Chemical shifts of VT-^{1}H-NMR with their respective FWHM of Figure 12

Nr.	T	β-H	FWHM β-H	phenyl-H	FWHM phenyl-H	axial-H	FWHM axial-H	other
	[°C]	[ppm]	[Hz]	[ppm]	[Hz]	[ppm]	[Hz]	[ppm]
1	- 40	9.27	10	8.38	15	-	-	7.33
				7.92	25	-	-	-

Nr.	T	(I+ II)	FWHM (I + II)-H	phenyl-H (III)	FWHM phenyl-H	axial-H (IV + V)	FWHM axial-H	other
	[°C]	[ppm]	[Hz]	[ppm]	[Hz]	[ppm]	[Hz]	[ppm]
2	- 40	13.73 (brs)	83	6.38	24	- 0.76 (s)	39.50	4.55
		7.23 (brs)	133	6.21	28	- 2.02 (s)	167.93	-
		-	-	5.28	-	- 8.46 (s)	-	-
3	- 20	12.32 (s)	32	6.40	36	- 0.66 (s)	29.45	4.55
		7.25 (brs)	123	6.22	28	- 1.58 (s)	38.11	-
		-	-	5.31	45	-8.11 (brs)	178.41	-
4	0	11.83 (s)	50	6.40	33	-0.55 (s)	15.07	4.55
		7.22 (brs)	128	6.23	20	-0.97 (s)	35.17	-
		-	-	5.36	33	-6.22 (brs)	178.41	-
5	22	11.44 (brs)	43	6.40	29	-0.546	34.27	4.55
		7.22 (brs)	92	6.23	27	-6.22	55.21	-
		-	-	5.36	26	-	-	-

The NMR of paramagnetic systems differs from diamagnetic systems in 3 notable ways:

    I.   the chemical shift scale

    II.   spectral line broadening and

    III.   T-dependence

Proton relaxation is strongly depended on intermolecular interactions and is therefore diffusion-controlled. The relaxation time (T_1) is normally around 10 s and line widths of 1 Hz or less are detected. In the presence of paramagnetic substances however the relaxation times are much shorter because T_1 is inversely proportional to the square magnetic moment (μ_{eff}) (Equation 5) and the magnetic moment of an unpaired electron is about a factor of 10^3 larger than the nuclear magnetic moment resulting in line widths up to several hundred hertz. [52,53]

$$\frac{1}{T_1} \sim \mu_{eff}^2$$

Equation 5 Relation of relaxation time to nuclear magnetic moment

T_1 .... Relaxation Time [s]
μ_{eff} .... Effective Nuclear Magnetic Moment [J/T]

    Therefore, it can be stated that hydrogen atoms exhibiting ^{1}H-NMR shifts with larger FWHM, as listed in Table 1 are in closer proximity to the suspected radical anion.
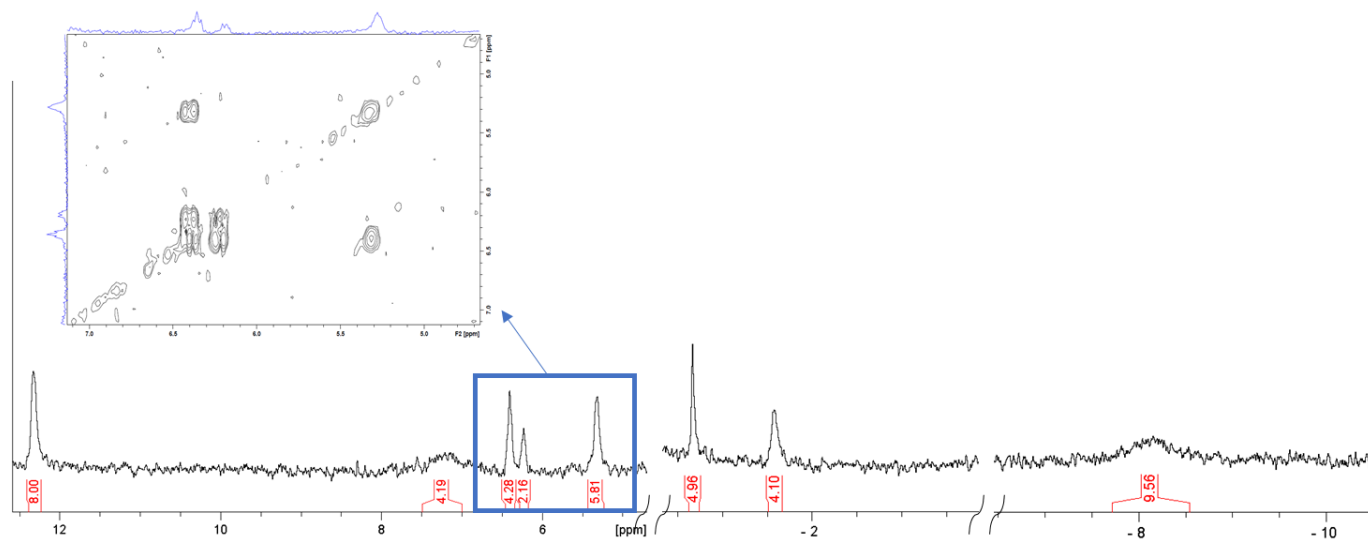
Figure 13 ^{1}H-NMR of the reaction mixture at -20 °C in THF-d8

For further evaluation the ^{1}H-NMR of the reaction mixture at -20 °C is displayed in Figure 13. Although the integrals are displayed, there is no information on whether they can be used due to the strong line broadening of the shifts. The shifts referring to the axial positions of porphyrins occur at -0.66 ppm, -1.58 ppm and -8.11 ppm. The correlation between the polar distance (R) to the incremental chemical shift ($\Delta\delta$) as described in 3.1.1 can unfortunately not be applied, since no investigations for R shorter than 2.74 Å (Sn-OH) have been made and applicability to paramagnetic species is unknown. It can however be concluded that the $\Delta\delta$ Sn-H for H_2SnTPP with R equal to the bond length (around 1.70 Å) is larger than 8 ppm. [54] Considering this it can be suggested that the shift at -8.11 ppm might refer to axial Sn-H hydrogen atoms. The shifts at -0.66 ppm and -4.10 ppm are in the typical range for alkoxides in axial position. [55] It might therefore be possible that these shifts can be assigned to THF in axial position, especially since it is reported that THF can coordinate to Sn(II) porphyrins. [46] To investigate this further a ^{1}H-NMR spectrum of the reaction in deuterated toluene should be measured.

The shifts at 6.40 ppm, 6.22 ppm and 5.31 ppm can be interpreted as phenyl-groups due to the H, H-COSY coupling. Usually the phenyl group shifts of tin tetraphenyl porphyrins occur around 7- 8.5 ppm, therefore the alleged phenyl group displayed in Figure 13 is high field shifted.

The shift at 12.32 ppm, which is suggested to be the resonance for the β-hydrogen atoms is in contrast to the alleged phenyl group low field shifted.

Due to the lack of information on paramagnetic NMR of porphyrins however, the assumptions stated cannot be further verified.

3.2.2 UV/VIS Spectroscopy

Figure 14 compares the UV/VIS spectra of the supposed radical species (red) to the educt Cl_2SnTPP (purple) and to the end product Sn(II)TPP (green), which are also listed in Table 2. Most porphyrin radical anions, as found via electrochemical studies, exhibit broad UV/VIS absorptions between 700 and 900 nm. [51,56,57] Thus, the bands at 705 nm and 898 nm substantiate the presumption that a radical anion species is present.
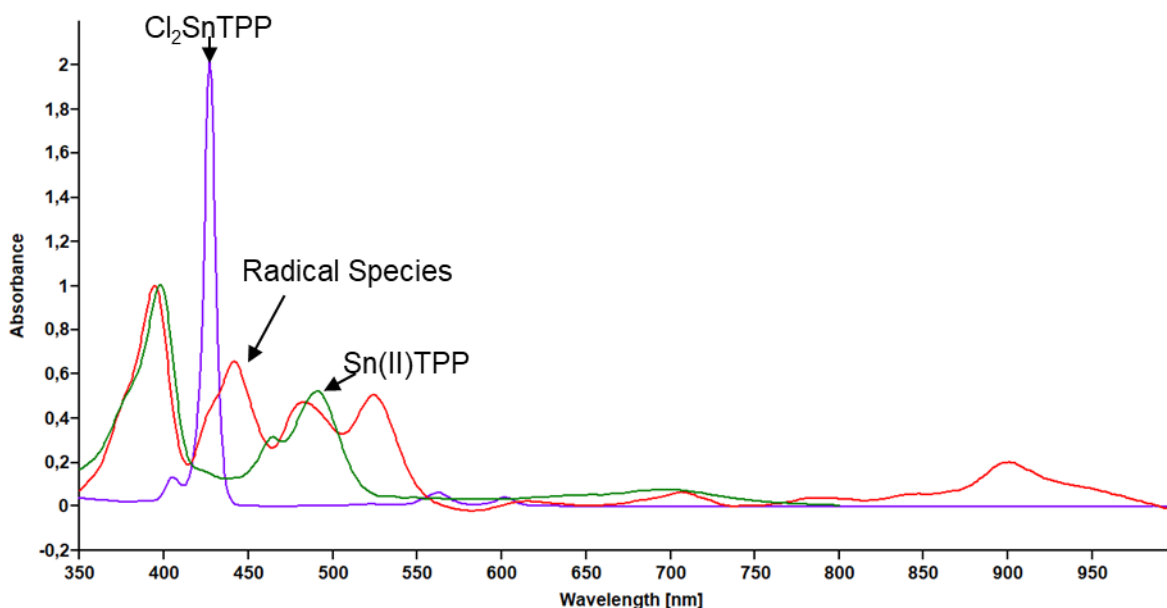
Figure 14 UV/VIS spectrum of Cl_2SnTPP (purple), the radical species (red) and Sn(II)TPP (green) in THF

The bands at 393 nm and 481 nm of the radical species are similar to the bands of Sn(II)TPP at 397 nm and 490 nm, which could suggest a Sn(II)TPP radical anion species.

Table 2 UV/VIS data of Figure 14

Porphyrin	Soret Band [nm]			Q Band [nm]		
Cl_2SnTPP	405	427	-	522	562	601
Radical species	393	442	481	523	705	898
Sn(II)TPP	397	463	490	-	-	695

3.2.3 EPR Spectroscopy

To counter check the presence of radicals as mentioned before EPR measurements were conducted. The EPR spectrum seen in Figure 15 consists of two broad peaks (peak-to-peak width ~9 gauss) of different intensity. The first peak with a g-factor of 2.0026 is similar to the g-factor observed for TPP radical anion species which exhibit g-factors in the range of 2.0026 - 2.0030. [49]
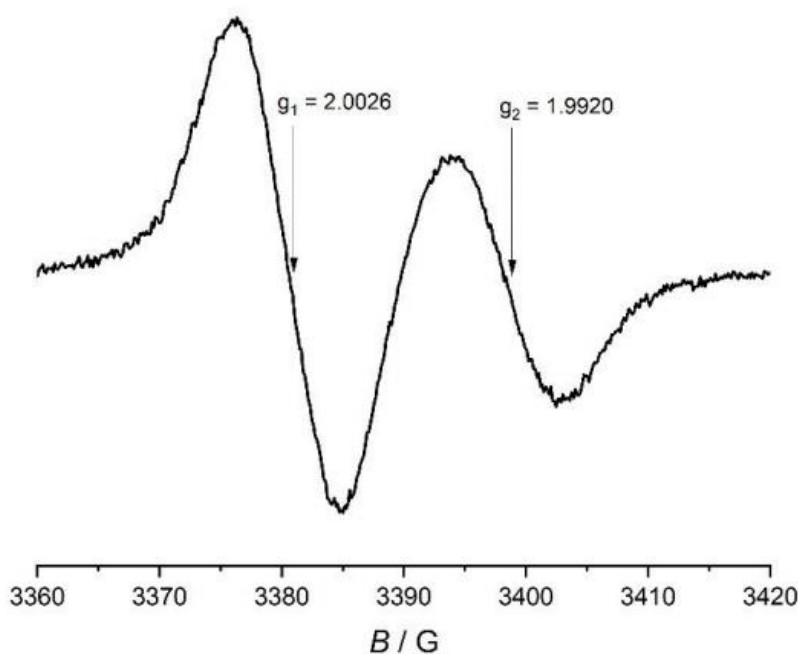
Figure 15 EPR spectrum of the reaction solution in THF at RT

Table 3 lists the parameters extracted from Figure 15. The g-factor was calculated according to Equation 6.

$$g = \frac{h\upsilon}{\mu_B B_0}$$

$$g = \frac{6.626 * 10^{-34} \frac{J}{s} * 9.474 * 10^9 Hz}{9.274 * 10^{-24} \frac{J}{T} * 0.338\ T}$$

$$g = 2.0026$$

Equation 6 Calculation of the g-Factor demonstrated on peak 1

Table 3 Parameters from EPR spectrum shown in Figure 15

Peak	g-Factor	ΔB_{pp} [Gauss]
1	2.0026	8.6
2	1.9920	8.8

Additionally, a second sample was investigated by EPR spectroscopy over a course of 3 hours as seen in Figure 16. The second peak vanishes after 3h after measuring the first EPR spectrum, while the first peaks takes on intensity. During this time a colour change from purple to green was detected.
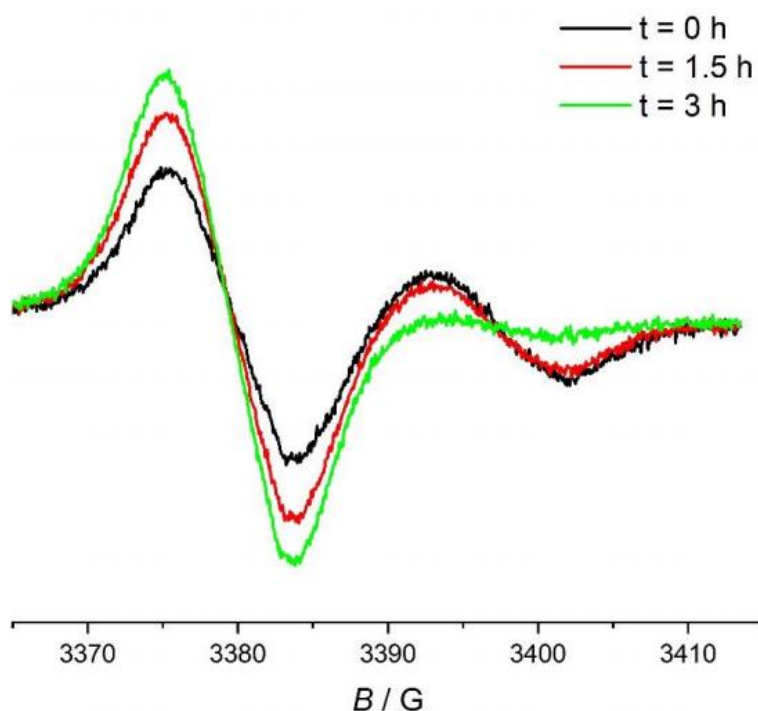
Figure 16 EPR spectrum of the reaction solution over a course of 3h in THF at RT

This suggests that two different radical porphyrin species are present in the reaction mixture. With the information's gathered via ^{1}H-NMR, UV/VIS and EPR it can be concluded:

o   at least two radical species exist

o   one is a radical anion situated in the porphyrin ring system and increases over time

o   the second radical species is unknown and unstable

Additionally, it is likely that the second radical species turns into the first one as seen in Figure 16.

However further investigations have to be conducted.

3.3 Influence of Dynamic Effects on the ¹H-NMR of Sn(II)TPP

As described in chapter 3.2 the reduction of Cl_2SnTPP with $LiAlH_4$ leads to Sn(II)TPP over intermediate radical species (see Scheme 3).
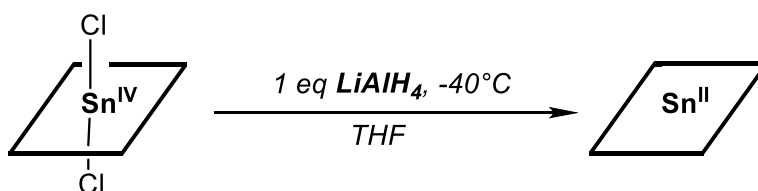
Scheme 3 Reaction of Cl_2SnTPP with $LiAlH_4$ yielding $Sn^{II}TPP$
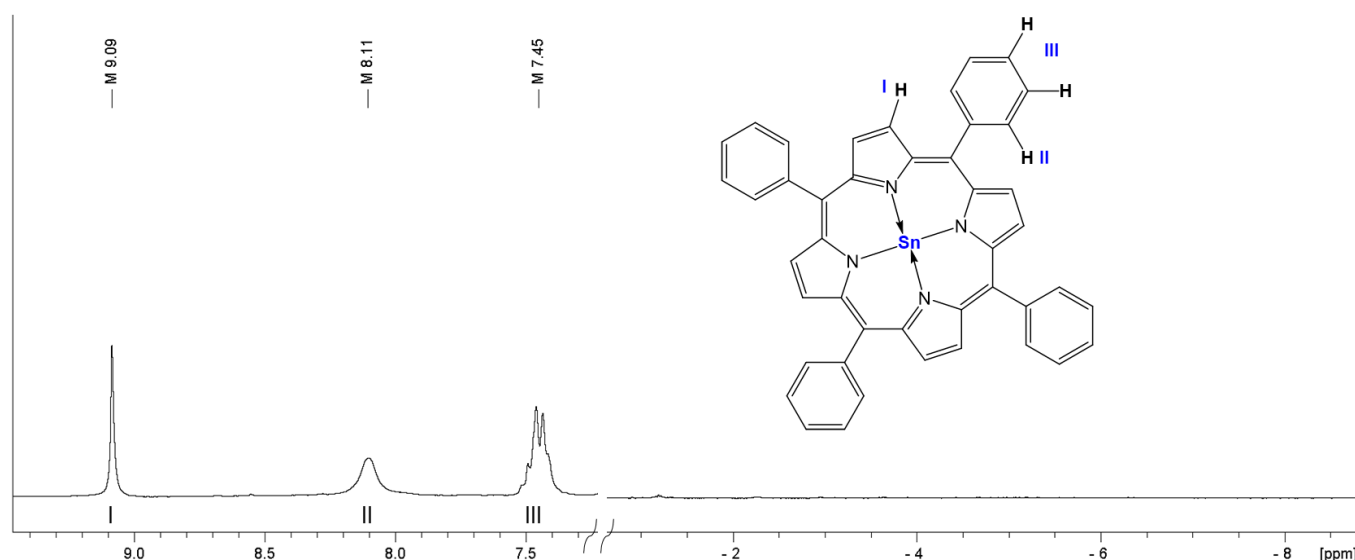
Figure 17 ¹H-NMR of Sn(II)TPP in C_6D_6

The ¹H-NMR of Sn(II)TPP is displayed in Figure 17. The hydrogen atoms of the macrocycle are labelled I to III and assigned to their respective resonances in the NMR. Unlike tin(IV) porphyrin species the ortho hydrogen atoms are displayed as a broad singlet rather than a doublet.

In solid state, as evidenced via crystallographic data of $Sn^{II}OEP$ (OEP= octaethylporphyrin), the tin atom shows an out-of plane displacement. Assuming that this out-of plane displacement of the tin atom is also valid in liquid state a splitting of the ortho proton shift due to the nonequivalence of both sides of the porphyrin cycle is therefore expected. At room temperature however no splitting of the *ortho*-H atoms is observed as displayed in Figure 17. [46] Guilard et al. described the influence of the temperature on the ¹H-NMR tin(II) tetra-*p*-tolylporphyrin in toluene-d_8 for a

temperature range of -20 °C to 40 °C. [46] Eaton et al. attributed this induced equivalence of the *ortho*-H atoms to the free rotation of the phenyl rings. [46,58] However as demonstrated recently in literature [16] for asymmetric substituted Sn(IV) porphyrins, the rotation of the phenyl rings is slow enough to split the *ortho*-H atoms into two equivalent signals. This suggests that the equivalence of the *ortho*-H of Sn(II)TPP is not a consequence of the phenyl ring rotation but caused by an interchanging position of the Sn(II) atom. Figure 18 displays the ^{1}H-NMR spectra of Sn(II)TPP in THF-d_8 at different temperatures ranging from -40 °C to 22 °C and of Cl_2SnTPP at -40 °C (1) as reference.
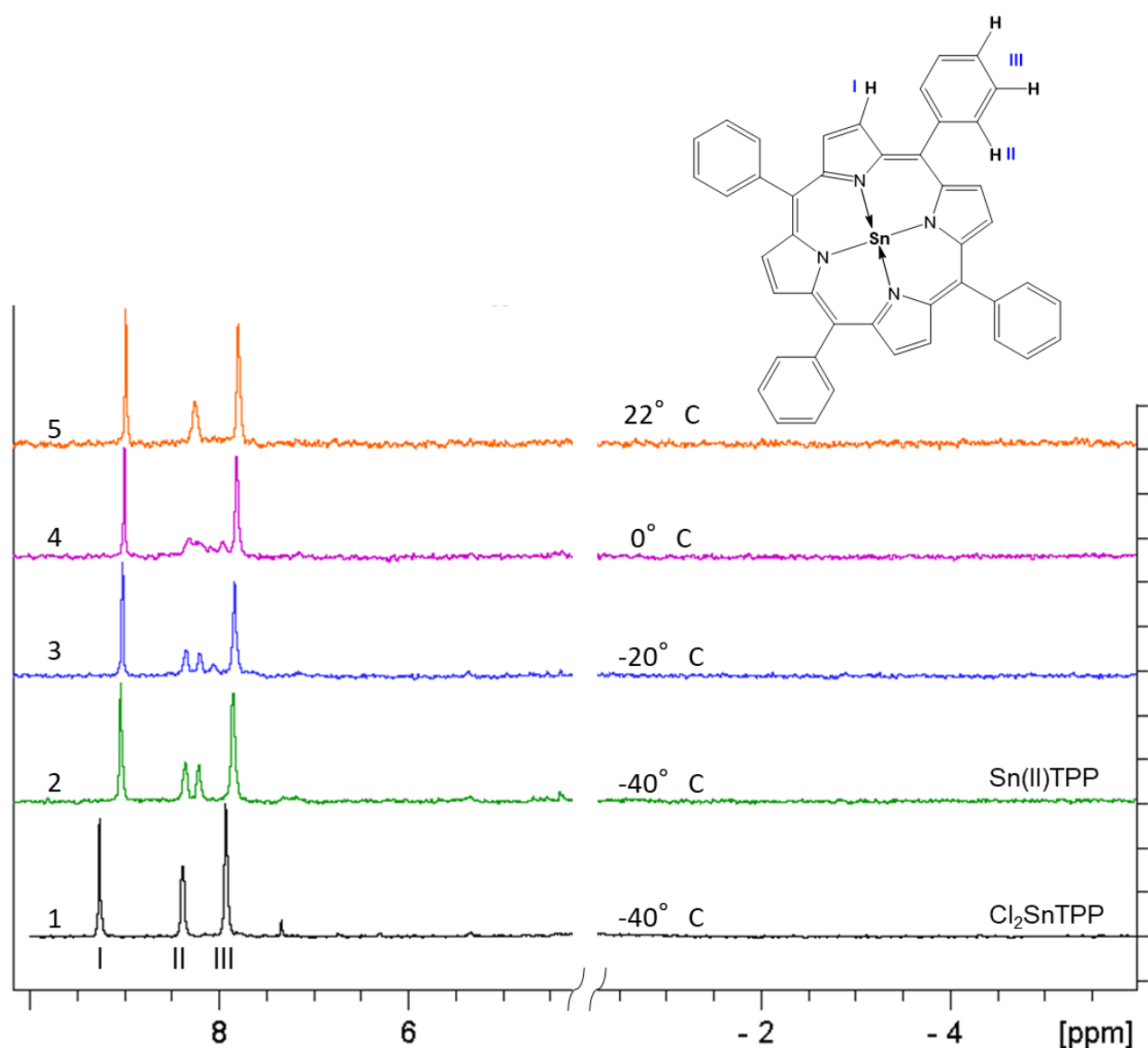
Figure 18 ^{1}H-NMR of Sn(II)TPP at various temperatures (2-5) and the 1H- NMR of Cl_2SnTPP (1) in THF-d_8

The ^{1}H-NMR shifts are listed in Table 4. At -20 °C (3) and -40 °C (2) two separate resonance signals are observed at 8.33 ppm and 8.19 ppm. As the temperature is raised to 0 °C (4) the signals broaden and start to coalesce to a single peak. The coalescence temperature is roughly between 0 °C and 10 °C, which correlates with the measurements of [46]. At 22 °C (5) the *ortho*-H resonance appears as a broad singlet at 8.24 ppm.

Table 4 Chemical shifts of spectra displayed in Figure 18

Nr.	T [°C]	β-H [ppm]	*o*-H [ppm]	*o*-H [ppm]	δυ [Hz]	*m-p*-H [ppm]	other [ppm]
1	- 40	9.27	8.38	-	-	7.33	-
2	- 40	9.02	8.33	8.19	44.62	7.82	-
3	- 20	9.00	8.33	8.19	45.18	7.82	8.05
4	0	9.00	8.32 – 8.17	-	34.90	7.82	7.94
5	22	8.97	8.24	-	-	7.78	-

The correlation between the ^{1}H-NMR spectrum and the kinetics of the Sn(II) displacement can also be estimated quantitatively. The following equations were drawn from NMR Spectroscopy: Basic Principles, Concepts and Applications by Harald Günther. [53]

The latter calculations are only an estimation of the kinetic process investigated in this variable temperature NMR study. The coalescence temperature as mentioned above is roughly between 0 °C and 10 °C, however no NMR spectra was measured at this temperature. Therefore, all further calculations adopt 0 °C as the coalescence temperature.

The rate constant $\kappa_{coal.}$ at the coalescence temperature T_c (K) for the exchange of two equally populated sites ($p_a = p_b$) can be calculated via Equation 7.

The frequency difference was determined for the proton NMR at -40 °C and -20 °C as demonstrated in Figure 19. The mean value of $\delta \upsilon$ at -40 °C and – 20 °C as listed in Table 4 was determined and used for further calculations.
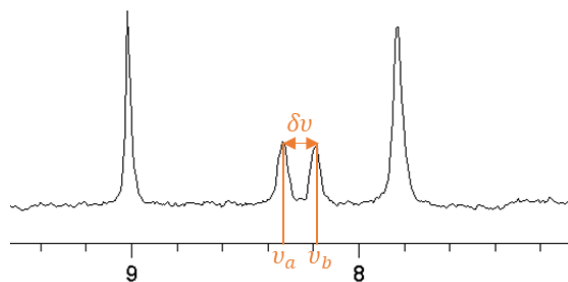
Figure 19 Determination of δv demonstrated through the ^{1}H-NMR of Sn(II)TPP at -40 °C

$$\kappa_{coal.} = \frac{\pi \delta v}{\sqrt{2}} = 2.22 \delta v$$

$$\kappa_{coal.} = \frac{\pi \delta v}{\sqrt{2}} = 2.22 * 44.9$$

$$\kappa_{coal.} = 99.7 \; s^{-1}$$

Equation 7 Rate constant $\kappa_{coal.}$ at the coalescence temperature T_c

δv .... Frequency difference $v_a - v_b$ in Hz

The rate constant at 0 °C is 99.7 s^{-1}. With this information the duration of the Sn(II) displacement at this temperature can be calculated through Equation 8.

$$\tau = \frac{1}{\kappa_{coal.}}$$

$$\tau = \frac{1}{99.7}$$

$$\tau = 0.01 \; s$$

Equation 8 Duration of the Sn(II) displacement

τ .... Duration of the Sn(II) displacement [s]

Moreover a quick evaluation of the energy barrier of this process at the coalescence temperature is enabled by the simplified Eyring equation (Equation 9).

$$\Delta G^{\ddagger} = RT_c \left[22.96 + \ln\left(\frac{T_c}{\delta v}\right) \right]$$

$$\Delta G^{\ddagger} = 8.314 * 273.15 \left[22.96 + \ln\left(\frac{273.15}{44.9}\right) \right]$$

$$\Delta G^{\ddagger} = 56242 \frac{J}{mol} = 56.242 \frac{kJ}{mol}$$

Equation 9 Eyring equation

$\Delta G^{\ddagger}$ .... Free energy of activation [J/mol]

R .... Gas constant [J/K*mol]

T_c .... Coalescence Temperature [K]

At 0 °C the free energy of activation for the Sn(II) displacement is 56.24 kJ/mol. The activation energy of aromatic ring rotation however is only about 13 kJ/mol. [59]

3.4 Possible Metal Exchange through Diisobutylaluminum- Hydride

While the reaction of Cl_2SnTPP with DIBAL at -40 °C yields almost exclusively Sn(II)TPP, carrying out the reaction at room temperature lead to rather unexpected shifts in the ^{1}H-NMR spectra as displayed in Figure 20. In general, 4 different porphyrin species could be determined through the shifts of the β-hydrogen atoms. Taking a closer look at the ^{1}H-NMR shifts associated with the axial ligands and the H, H-COSY of the corresponding region the shifts at -1.52 ppm (d), -2.50 ppm (hept) and -5.71 ppm (d) labelled a, b and c of Figure 20 can be identified as isobutyl in axial position.
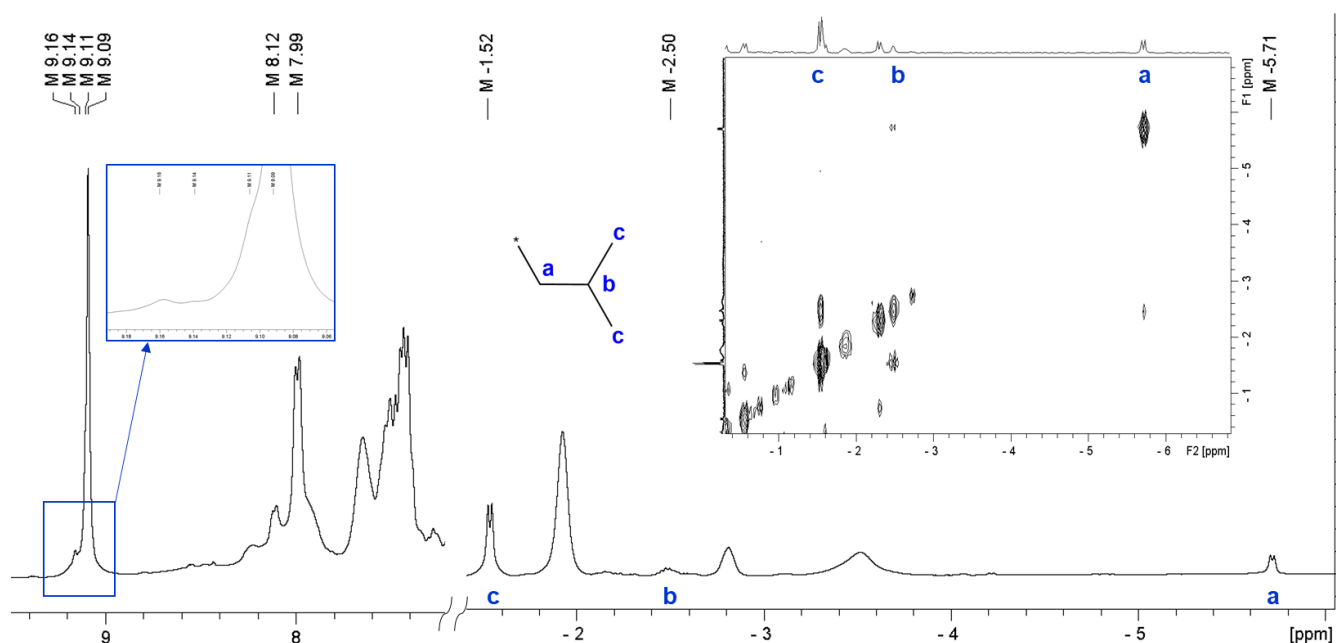
Figure 20 ^{1}H-NMR and H, H-COSY NMR of the reaction mixture of the reaction Cl_2SnTPP with DIBAL at RT in C_6D_6

To further verify the main product $(i\text{-Bu})_2SnTPP$ was prepared for comparison via the reaction of Cl_2SnTPP with 2 eq $i\text{-BuMgBr}$ (Scheme 4) similar to the reaction published by Cloutour et al. [60]
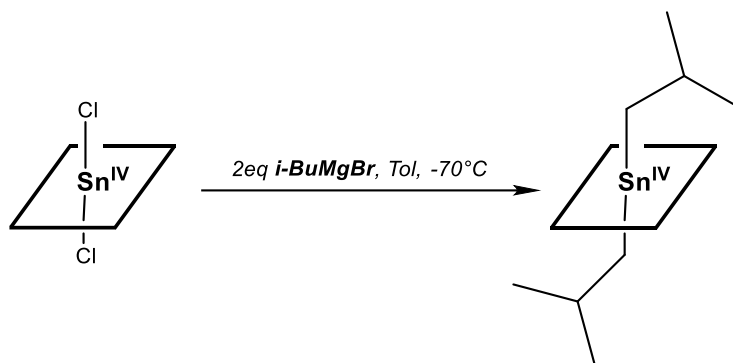
Scheme 4 Reaction of Cl_2SnTPP with i-BuMgBr yielding (i-Bu)$_2$SnTPP

Figure 21 displays the ^{1}H-NMR and H, H-COSY NMR of this reaction. The shifts referring to the axial region at -1.95 (d), -3.98 (hept) and -6.49 (d) exhibit the same multiplicity and coupling in the H, H-COSY NMR but not the same chemical shift.
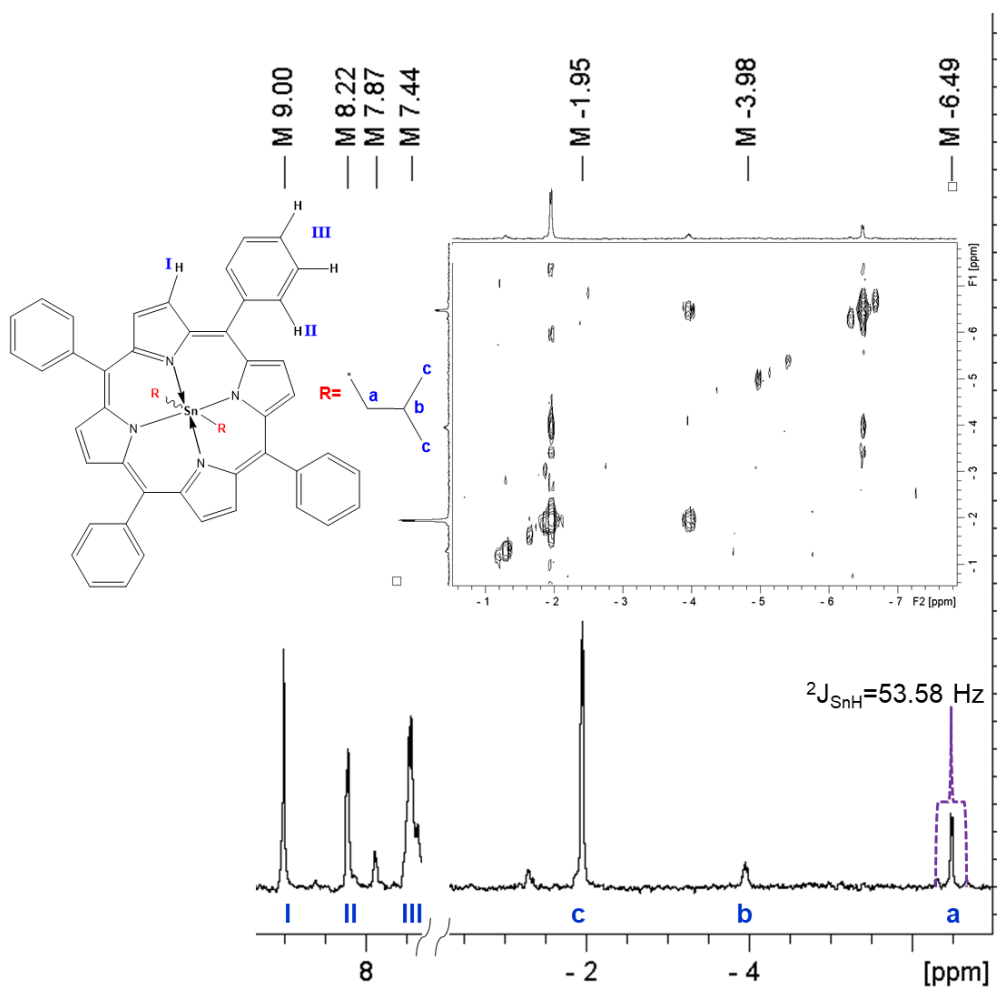
Figure 21 ^{1}H-NMR and H, H- COSY NMR of (i-Bu)$_2$SnTPP in C_6D_6

Furthermore, contrary to Figure 21, which exhibits a $^2J_{SnH}$ coupling constant of 53.58 Hz, no $^2J_{SnH}$ coupling was detected in the ^1H-NMR of Figure 20. Therefore, the following reaction as displayed in Scheme 5 is proposed.
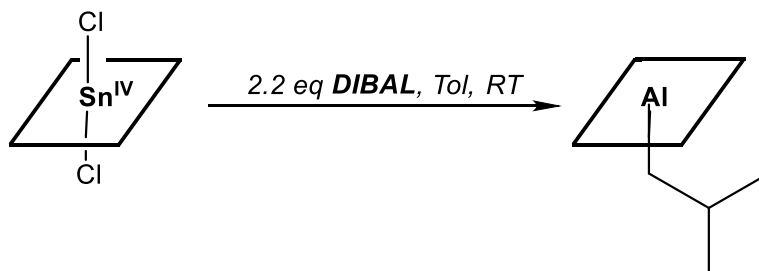
Scheme 5 Reaction of Cl₂SnTPP with DIBAL yielding supposedly "*i*-BuAlTPP"

Table 5 and Table 6 compare the ^1H-NMR and UV/VIS data of the supposed *i*-BuAlTPP with the literature known *n*-BuAlTPP [61] and (*i*-Bu)₂SnTPP. The α-CH$_2$ of the isobutyl chain of (*i*-Bu)₂SnTPP at -6.49 ppm is more low-field shifted than α-CH$_2$ of *n*-BuAlTPP at -5.63 ppm. A possible reason is the distance of the metal from the porphyrin plane. The tin atom of Sn(IV) porphyrins is located in the porphyrin plane. [17] Aluminum however as crystallographic data of (OEP)Al(CH₃) shows is 0.47 Å displaced from the plane of the four nitrogen atoms, whereas α-CH$_2$ is affected slightly different by the π-ring current leading to a different chemical shift. [61]

Table 5 Comparison of the ^1H-NMR of *n*-BuAlTPP, "*i*-BuAlTPP" and (*i*-Bu)₂SnTPP in C₆D₆

Porphyrin	β-H [ppm]	*o*-H [ppm]	*m-p*-H [ppm]	axial H [ppm]	$^2J_{SnH}$ [Hz]
***n*-BuAlTPP** [61]	9.11 (s)	8.10 (d)	7.44 (m)	-0.37 (tr) -1.06 (m) -2.89 (m) -5.63 (tr)	-
"*i*-BuAlTPP"	9.09 (s)	8.12 (d)	7.44 (m)	-1.52 (d) -2.50 (hept) -5.71 (d)	not observed
(*i*-Bu)₂SnTPP	9.00 (s)	8.22 (d)	7.44 (m)	-1.95 (d) -3.98 (hept) -6.49 (d)	53.58

The shifts referring to the axial H-atoms of *n*-BuAlTPP fit quite well to those of the supposed *i*-BuAlTPP. The UV/VIS spectra listed in Table 6 shows the same affinity between *n*-BuAlTPP and the supposed *i*-BuAlTPP. Only the first Q band of "*i*-BuAlTPP" at 490 nm does not fit the trend which might be indebted by the side products of this reaction. For closer comparison Et$_2$SnTPP was synthesized and by comparison of (*i*-Bu)$_2$SnTPP and Et$_2$SnTPP as listed in Table 6 proven that comparing the UV/VIS spectra of these compounds is legitimate as a result of the minor influence of the axial ligands (as long as it is of alkyl type) on the absorption behavior. [18] The supposed *i*-BuAlTPP clearly differs from these two alkyl tin porphyrins (see also Figure 22).

Table 6 Comparison of the UV/VIS spectra of *n*-BuAlTPP in benzene, "*i*-BuAlTPP" and (*i*-Bu)$_2$SnTPP in toluene

Porphyrin	Soret bands [nm]			Q bands [nm]	
n-BuAlTPP [61]	376	436	516	567	614
"*i*-BuAlTPP"	398	434	490	565	606
(*i*-Bu)$_2$SnTPP	432	456	568	617	667
Et$_2$SnTPP	429	455	564	622	662
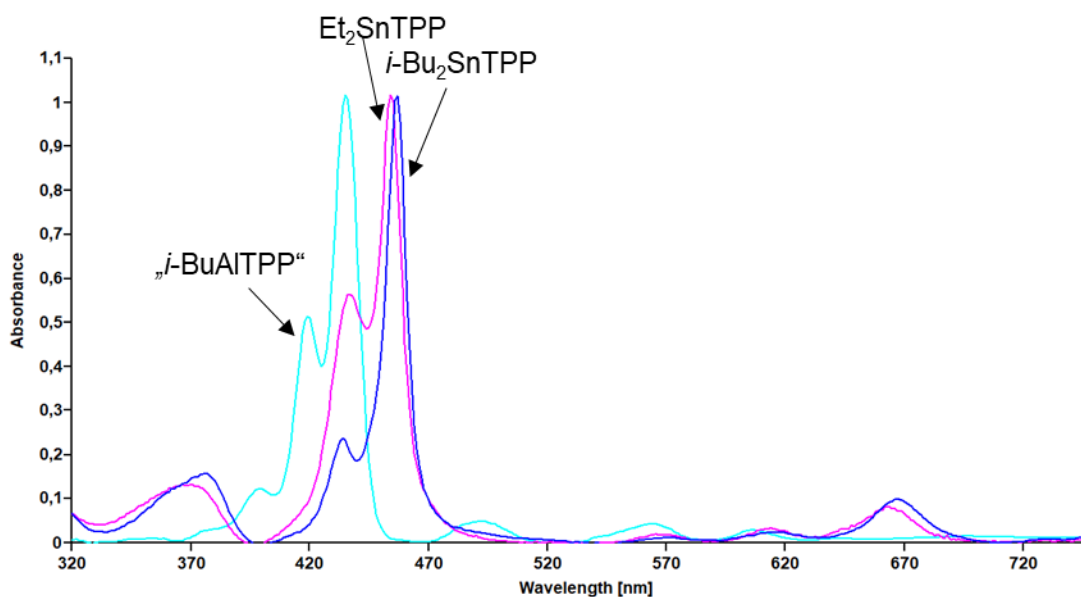
Figure 22 UV/VIS of "*i*-BuAlTPP" (turquise), (*i*-Bu)$_2$SnTPP (dark blue) and Et$_2$SnTPP (purple) in toluene

Nonetheless, to securely verify the synthesis of "*i*-BuAlTPP" and therefore proof the metal exchange of the tin porphyrin with DIBAL, the compound *i*-BuAlTPP should be synthesized via a different synthesis route and characterized for comparison however first attempts to synthesize *i*-BuAlTPP failed so far.

3.5 Synthesis and Characterization of H₂GeTPP

The attempt to synthesize H₂GeTPP was performed according to Scheme 6. During the reaction a colour change from purple (educt) to greenish/blue occurred immediately.
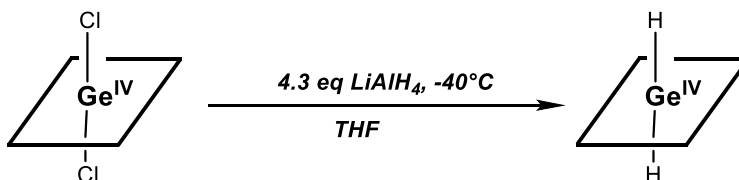
Scheme 6 Reaction of Cl₂GeTPP with LiAlH₄ yielding H₂GeTPP

3.5.1 ¹H-NMR of H₂GeTPP
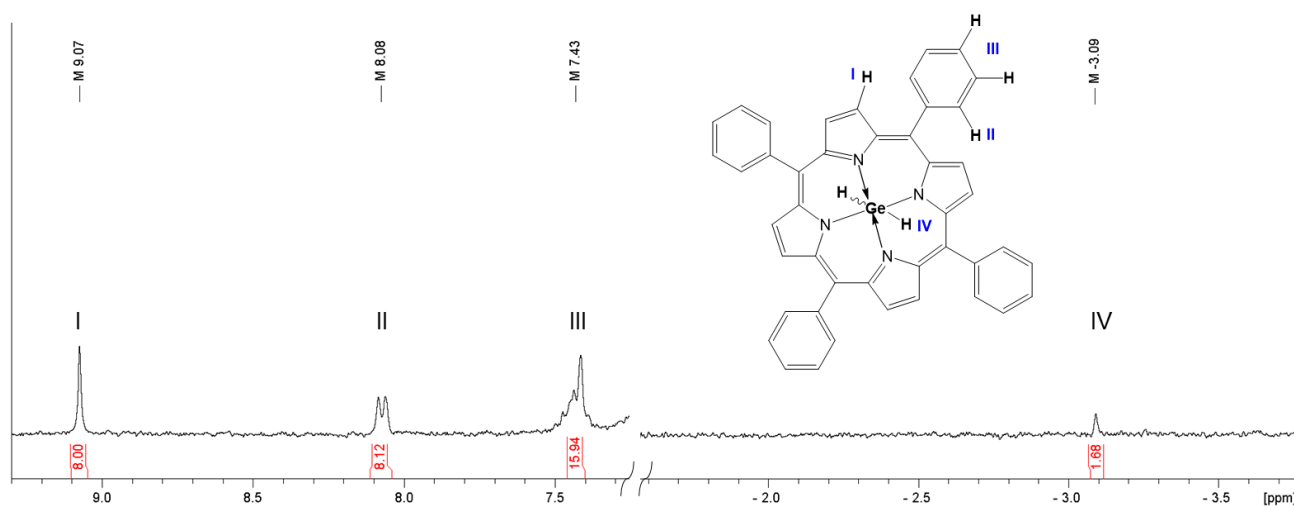
Figure 23 ¹H-NMR of alleged H₂GeTPP in C₆D₆

Figure 23 shows the ¹H-NMR of the compound in C₆D₆. The hydrogen atoms of the macrocycle are labelled I to III and the assumed signal for the axial hydrogen atom is labelled with IV. The integral ratio of I vs IV is 8 : 1.68, which also fits the assumption.

The reaction was investigated via VT-¹H-NMR from -40 °C to 22 °C as displayed in Figure 24. The chemical shifts are listed in Table 7. The ¹H-NMR of Cl₂GeTPP at -40 °C (1) is shown as a reference. It can be observed that the shifts are not temperature dependent. The shift of the axial hydrogen atoms occurs at -4.16 ppm (in THF-d₈). Spectra 3 and 4 show contamination with (HO)₂GeTPP due to a shift of low intensity at -6.36 ppm. [62]
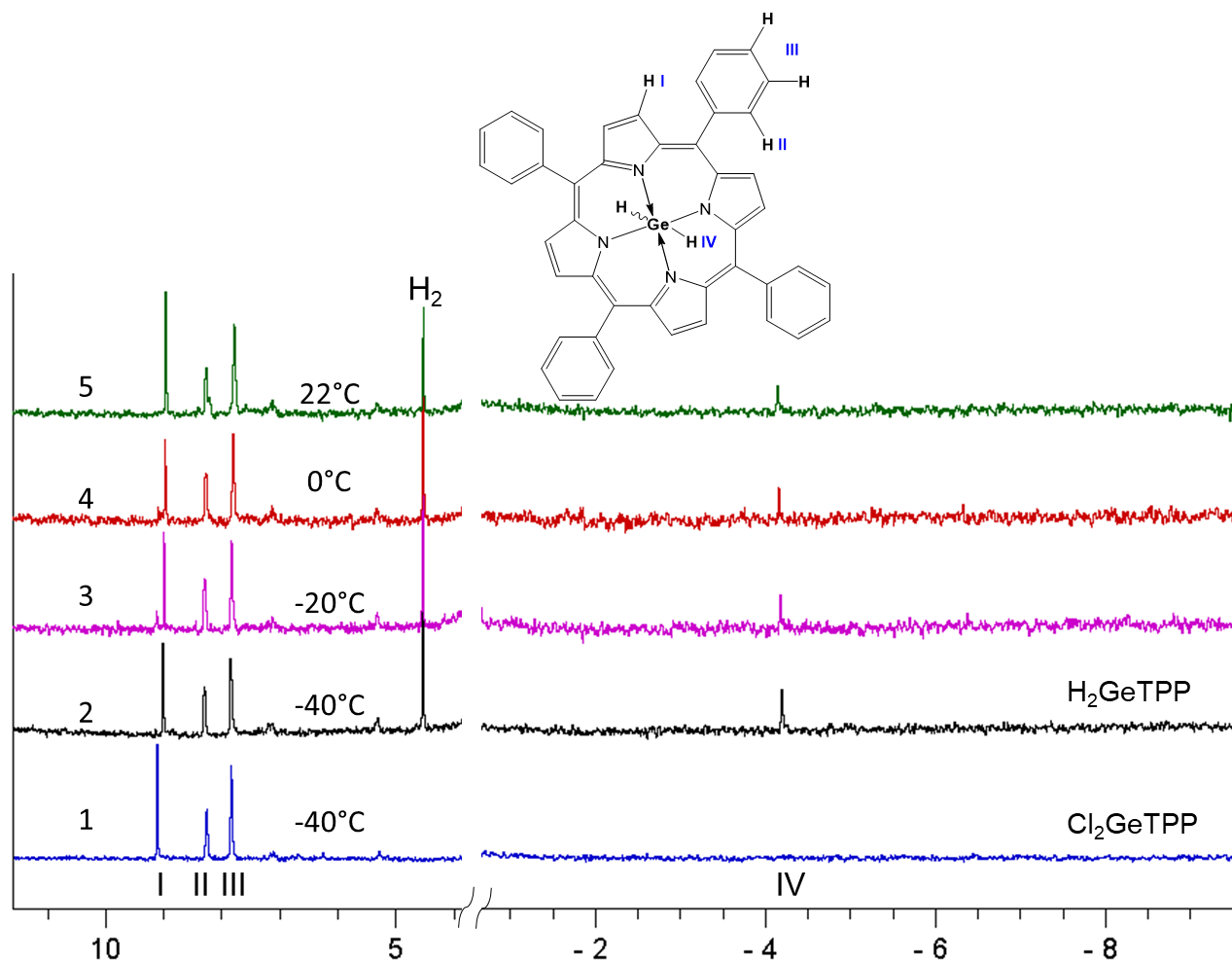
Figure 24 VT-NMR of H_2GeTPP from -40 °C to 22 °C (2-3) and Cl_2GeTPP (1) at -40 °C as reference in THF-d_8

Table 7 Chemical shifts of Figure 24

Nr.	T [°C]	β-H [ppm]	o-H [ppm]	m-p-H [ppm]	axial [ppm]	other [ppm]
1	- 40	9.16	8.31	7.87	-	-
2	- 40	9.02	8.31	7.87	- 4.20	4.55
3	- 20	9.01	8.30	7.84	- 4.16	4.55
		9.16				
4	0	8.97	8.27	7.8	- 4.16	4.55
		9.09				
5	22	8.95	8.26	7.77	- 4.16	4.55

The ^{1}H- NMR of H_2GeTPP was measured in THF-d_8 and C_6D_6. A comparison of the shifts is listed in Table 8.

Table 8 Comparison of the chemical shifts of H_2GeTPP in THF-d_8 with H_2GeTPP in C_6D_6

Solvent	T [°C]	β-H [ppm]	o-H [ppm]	m-p-H [ppm]	axial [ppm]
THF-d_8	22	8.95	8.26	7.77	-4.16
C_6D_6	22	9.07	8.07	7.43	-3.09

3.5.2   UV/VIS of H_2GeTPP

The UV/VIS spectra of H_2GeTPP and Cl_2GeTPP (as reference) are displayed in Figure 25 and listed in Table 9. Comparison of H_2GeTPP (428 nm, 454 nm) with Cl_2GeTPP (406 nm, 427 nm) shows a 22-27 nm red shift of the Soret-Band. Similar shifts are reported for C-bound germanium porphyrins such as Et_2GeTPP which exhibits a Soret-Band at 451 nm. [42]
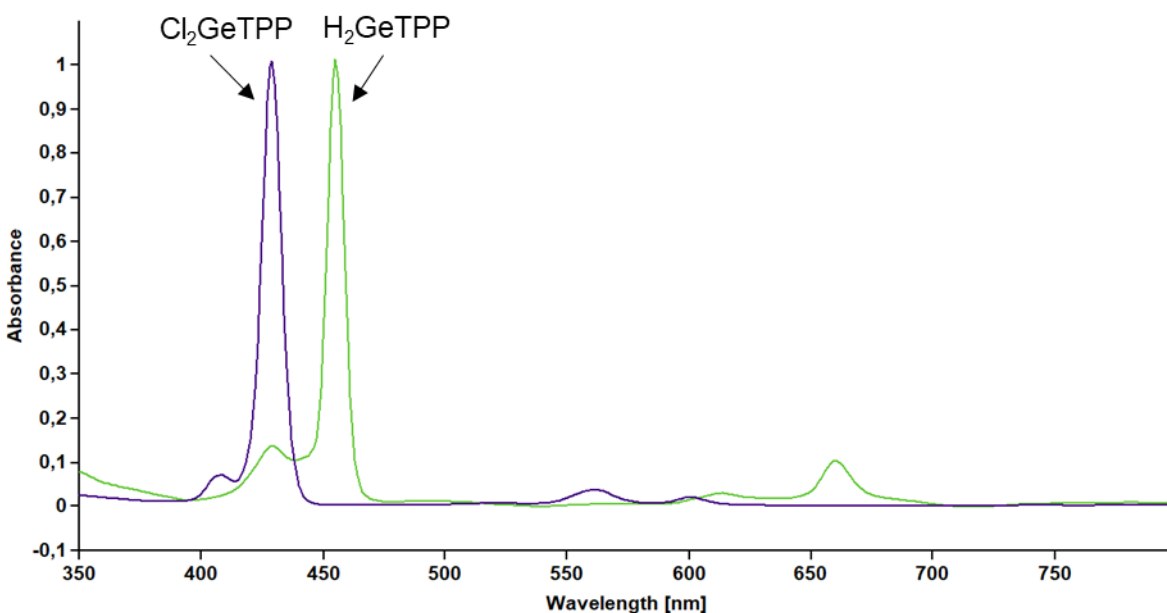
Figure 25 UV/VIS of Cl$_2$GeTPP (purple) in THF and H$_2$GeTPP (green) in C$_6$D$_6$

Table 9 Comparison of the UV/VIS spectra of Cl$_2$GeTPP and H$_2$GeTPP displayed in Figure 25

	Soret-Band [nm]			Q-Band [nm]	
Cl$_2$GeTPP	406	427	517	561	600
H$_2$GeTPP	428	454	-	612	659
Et$_2$GeTPP [42]	-	451	558	603	650

3.5.3 ATR-FTIR

The alleged H$_2$GeTPP was measured via ATR-FTIR. A potential Ge-H vibration at 1961 cm^{-1} was detected as displayed in Figure 26. A Ge-OH vibration can be ruled out due to the reported value of 655 cm^{-1} for Ge-OH. [57] Compared to tetra-coordinated Ge-hydrides, at which the Ge-H vibration is detected at about 2060 cm^{-1} [63], the Ge-H vibration of the hexa-coordinated H$_2$GeTPP is shifted to lower wavenumbers. The C-H vibration of toluene was also detected at 2940 cm^{-1}- 2851 cm^{-1}.
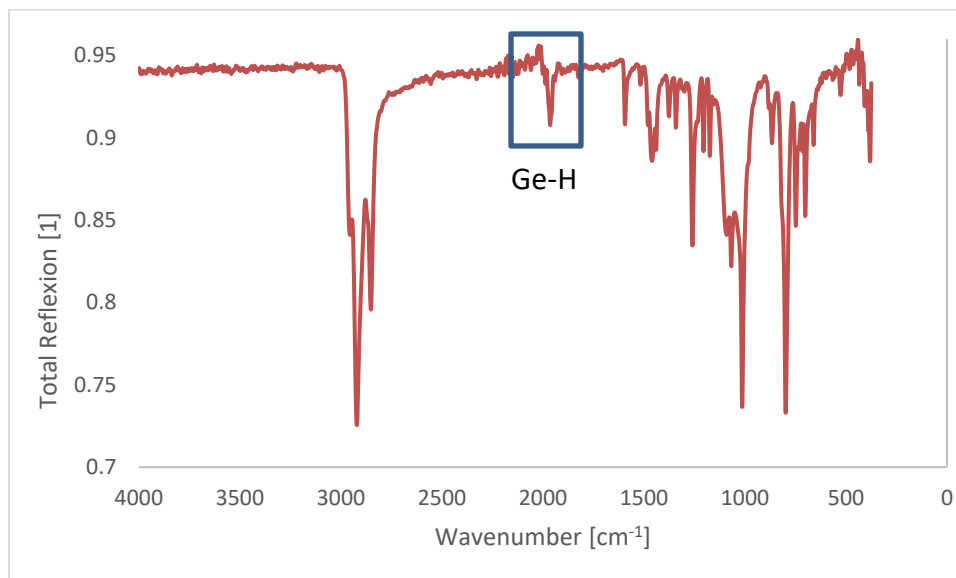
Figure 26 ATR-FTIR of H₂GeTPP

3.5.1 Stability of H₂GeTPP
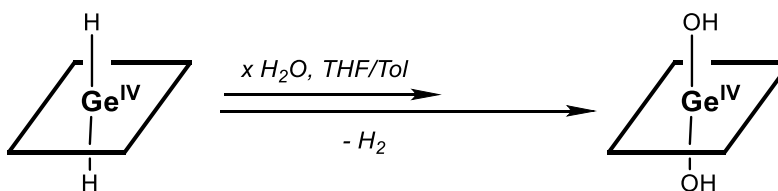
Scheme 7 Hydrolysis of H₂GeTPP to (HO)₂GeTPP

The alleged H₂GeTPP hydrolyses to (HO)₂GeTPP according to Scheme 7. During this reaction a color change from green to reddish/purple can be detected. This was evidenced by ^{1}H-NMR (shift at -6.72 ppm) and UV/VIS (see Figure 27, Figure 28 and Table 10).
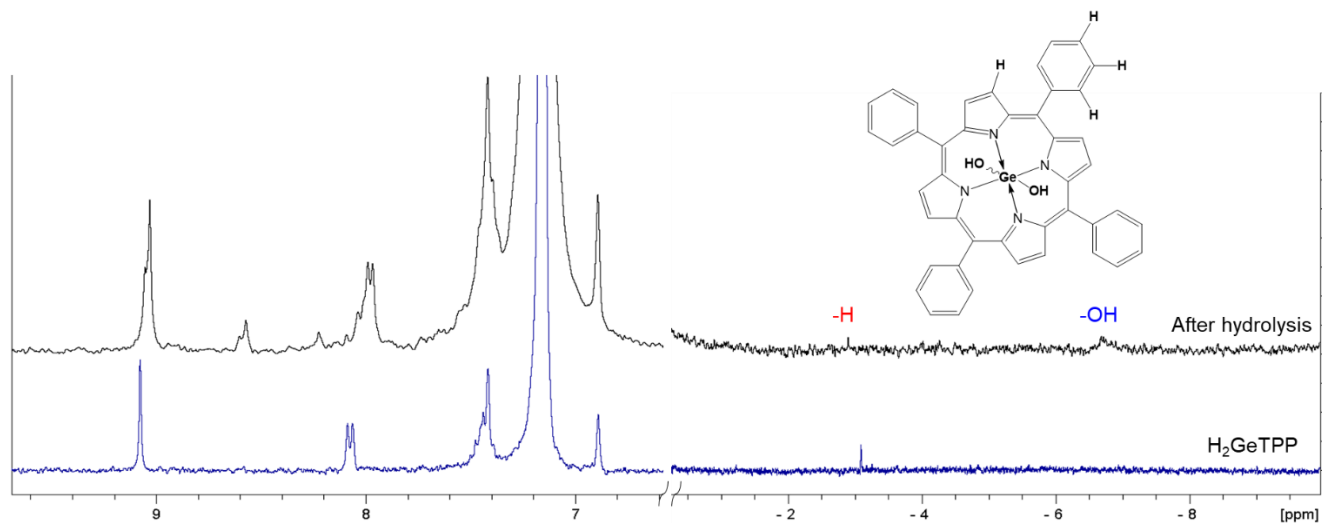
Figure 27 ^{1}H-NMR of H$_2$GeTPP (blue) and the reaction displayed in Scheme 7 (black)
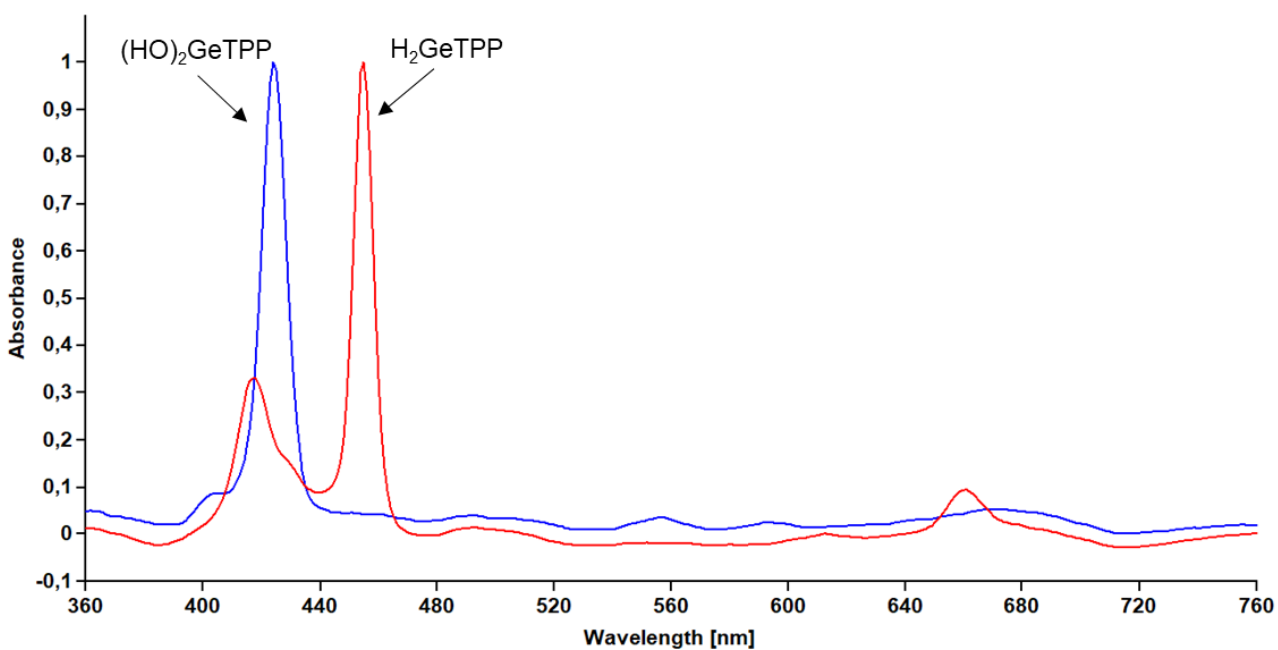
Figure 28 UV/VIS of the reaction seen in Scheme 7, (HO)$_2$GeTPP (blue), H$_2$GeTPP (red) in C$_6$D$_6$

Table 10 UV/VIS data of Figure 27 compared to the literature date of (HO)$_2$GeTPP [64] in PhCN

	Soret-Band [nm]		Q-Band [nm]		
(HO)₂GeTPP	403	425	513	557	595
(HO)₂GeTPP [64]	404	426	517	556	596
H₂GeTPP	428	454	-	612	659

3.6 Synthesis and Characterization of H$_2$SiTPP

Attempts to synthesize H$_2$SiTPP were performed according to Scheme 8. A color change from blueish/purple to green occurred in a matter of seconds.
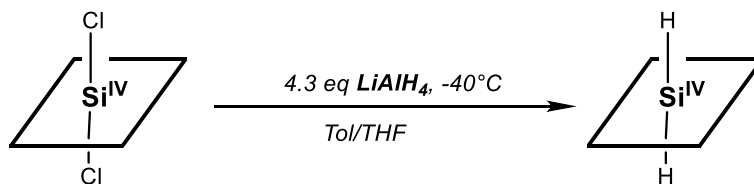
Scheme 8 Reaction of Cl$_2$SiTPP with LiAlH$_4$ yielding H$_2$SiTPP
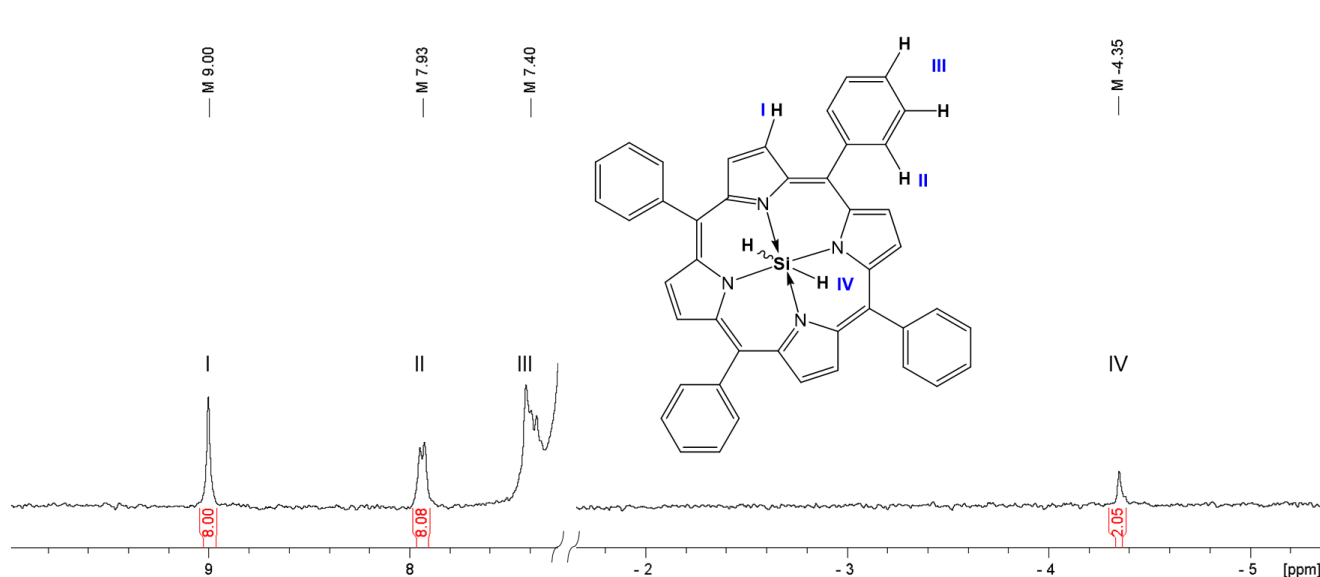
Figure 29 ^{1}H-NMR of alleged H$_2$SiTPP in C$_6$D$_6$

Figure 29 shows the ^{1}H-NMR of the alleged H$_2$SiTPP in C$_6$D$_6$. The integral ratio of the β-hydrogen atoms, *ortho*-hydrogen atoms and axial hydrogen atoms is 8 : 8.08 : 2:05, fitting the assumption.

Table 11 Comparison of the ^{1}H-NMR of H_2TPP and Cl_2SiTPP to H_2SiTPP in C_6D_6

Compound	T [°C]	β-H [ppm]	*o*-H [ppm]	*m-p*-H [ppm]	axial [ppm]
H₂TPP	22	8.93	8.11	7.46	-2.12
Cl₂SiTPP	22	8.85	7.76	7.29	-
H₂SiTPP	22	8.99	7.93	7.38	-4.36

Due to the low solubility of the alleged H_2SiTPP (<2 mmol/l in C_6D_6) and the low natural abundance of ^{29}Si, no ^{29}Si-NMR of this compound could be measured even after 2 days.

3.6.1 UV/VIS of H₂SiTPP

For better clarity the UV/VIS spectra of Cl_2GeTPP (blue, dotted), Cl_2SiTPP (pink), H_2GeTPP (light green, dotted) and H_2SiTPP (dark green) are shown in Figure 30 and listed in Table 12. H_2SiTPP exhibits a 25- 26 nm red shift of the Soret-band compared to Cl_2SiTPP, which fits the observed red shift of H_2GeTPP compared to Cl_2GeTPP as described in 3.5.2.

Table 12 Comparison of the UV/VIS spectra of Cl_2SiTPP and H_2SiTPP displayed in Figure 25

		Soret-Band [nm]		Q-Band [nm]	
Cl₂SiTPP	-	414	436	569	609
H₂SiTPP	419	439	462	626	673
Cl₂GeTPP	406	427	517	561	600
H₂GeTPP	428	454	-	612	659
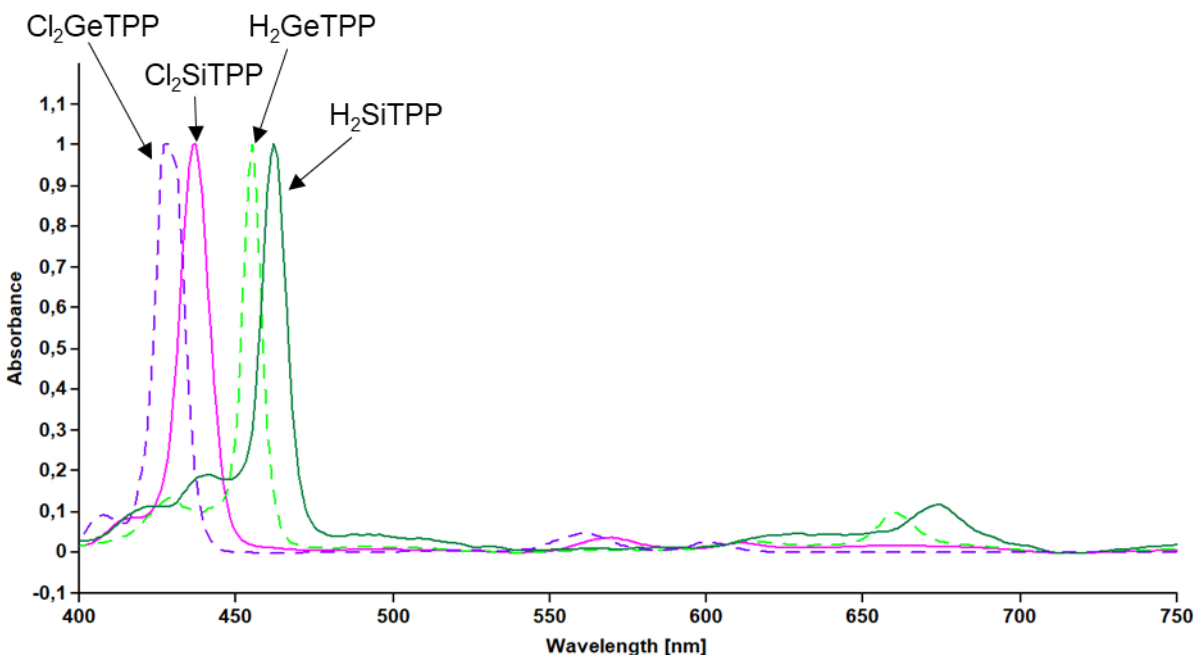
Figure 30 UV/VIS of Cl$_2$GeTPP (blue, dotted), Cl$_2$SiTPP (pink), H$_2$GeTPP (light green, dotted) and H$_2$SiTPP (dark green)

3.6.2 Stability of H$_2$SiTPP

H$_2$SiTPP reacts with traces of water analogous to the hydrolysis of H$_2$GeTPP according to Scheme 9 as evidenced by ^{1}H-NMR (shift at -6.75 ppm) and UV/VIS (Figure 31, Figure 32 and Table 13). To obtain the exact mechanism of the hydrolysis further investigations have to be conducted.
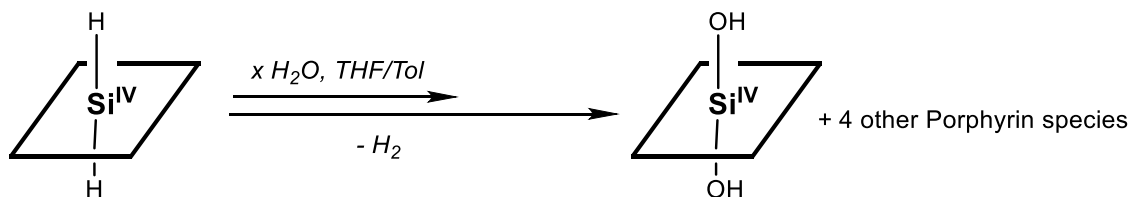
Scheme 9 Reaction of H$_2$SiTPP with H$_2$O to (HO)$_2$SiTPP
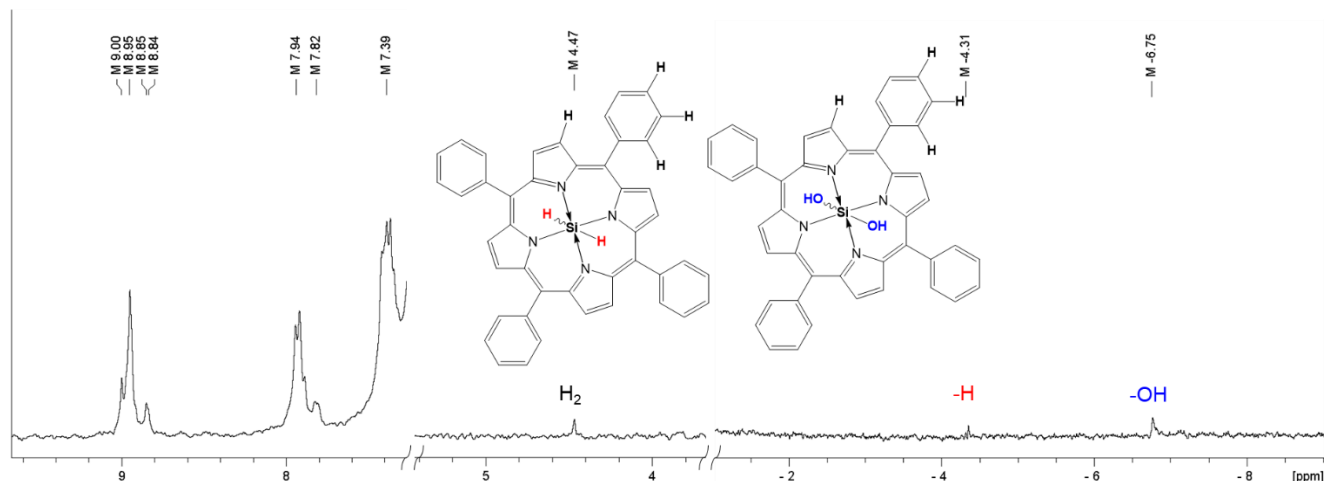
Figure 31 ^{1}H-NMR of the reaction seen in Scheme 9
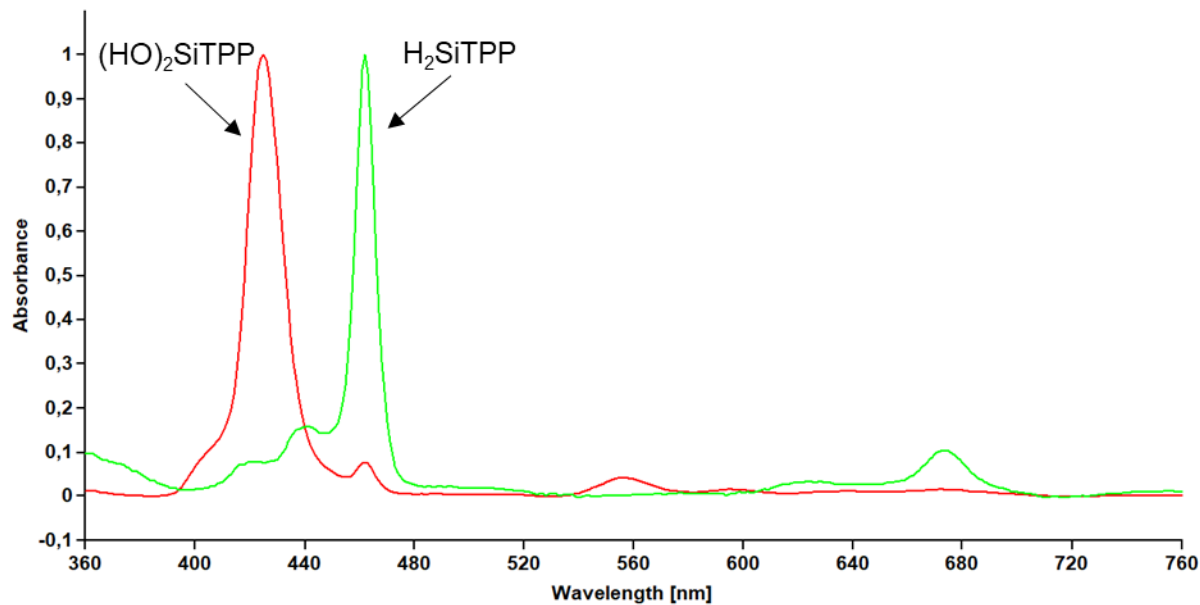
Figure 32 UV/VIS of the reaction seen in Scheme 9, (HO)$_2$SiTPP (red), H$_2$SiTPP (green) in C$_6$D$_6$

Table 13 UV/VIS data of Figure 32 compared with the literature known UV/VIS of (HO)$_2$SiTPP [65] in CHCl$_3$

	Soret-Band [nm]			Q-Band [nm]	
(HO)₂SiTPP	403	425	555	596	632
(HO)₂SiTPP [65]	-	424	555	597	-
H₂SiTPP	419	439	462	626	673

4 Summary & Outlook

Throughout this thesis we were able to show three new synthetic routes towards Sn(II)TPP via the reduction of Cl_2SnTPP with $LiAlH_4$, DIBAL and $K[BEt_3]H$ at -40 °C. The dynamic behaviour of the ^{1}H-NMR of the *ortho*-hydrogen atoms of Sn(II)TPP could also be displayed by VT-NMR. It was shown that the equivalence of the *ortho*-hydrogen atoms at room temperature does not originate from the phenyl ring-rotation but from the Sn(II) displacement. Therefore, the free energy of activation of 56.24 kJ/mol was calculated.

Furthermore, a possible metal exchange occurring at the reaction of Cl_2SnTPP with diisobutylaluminiumhydride at room temperature was observed.

The synthesis of H_2SnTPP was not possible due to the subsequent formation of Sn(II)TPP over two radical anion species evidenced by EPR spectroscopy. To resolve the exact reaction mechanism further investigations, have to be conducted.

However, attempts to synthesize H_2GeTPP were successful according to ^{1}H-NMR and ATR-FTIR. A red shift of 22- 27 nm in the UV/VIS compared to Cl_2GeTPP could be observed. The alleged H_2GeTPP subsequently hydrolyses to $(HO)_2GeTPP$.

Attempts to synthesize H_2SiTPP were also conducted and successful according to ^{1}H-NMR. H_2SiTPP also exhibits a red shift compared to Cl_2SiTPP. Analogous to H_2GeTPP the corresponding silicon compound hydrolyses to $(HO)_2SiTPP$. To verify the synthesis of these new compounds unambiguously characterisation via single-crystal x-ray diffraction is still pending.

5 Experimental Part

5.1 Materials and Methods

All reactions were carried out under the exclusion of water and air in a nitrogen or argon atmosphere using Schlenk techniques. All used glassware was dried three times prior to use. Solvents, unless mentioned otherwise were obtained by an Innovative Technology, Inc. solvent drying system. Purchased chemicals and their storage are listed in Table 14.

Table 14 Substances purchased, A= stored in air, I= inert atmosphere

Substance	CAS- Number	Purchased from	Storage
H_2TPP	917-23-7	abcr chemicals	A
$SnCl_2*2H_2O$	10025-69-1	Riedel-de Haën	A
$GeCl_4$	10038-98-9	abcr chemicals	I
NaH	7646-69-7	Sigma Aldrich	I
H_3B*THF 1M in THF	14044-65-6	Sigma Aldrich	I
DIBAL 1M in Tol	1191-15-7	Sigma Aldrich	I
$LiAlH_4$	16853-85-3	Acros Organics	I
$K[BEt_3]H$ 1M in THF	22560-21-0	Sigma Aldrich	I
$ZnEt_2$ 1M in Hexane	557-20-0	Sigma Aldrich	I
i-BuMgBr 2M in Et_2O	926-62-5	Sigma Aldrich	I

5.2 NMR Spectroscopy

All NMR measurements were carried out by the "Varian Mercury 300" with a resonance frequency of 300 MHz for ^{1}H-NMR and 111,8 MHz for ^{119}Sn-NMR. The chemical shifts were recorded in ppm (parts per million) relative to TMS for ^{1}H-NMR and Me_4Sn for ^{119}Sn-NMR. Multiplicity is mentioned with the abbreviations s, d, t, hept and m for singlet, doublet, triplet,

heptet and multiplet. The samples were filled into NMR tubes with a diameter of 5 mm under inert atmosphere and sealed with parafilm. As a solvent dry C_6D_6 or dry THF-d_8 were used. C_6D_6 was dried over P_4O_{10} and distillation. THF-d_8 was dried over potassium and distillation.

5.3   UV/VIS Spectroscopy

All UV/VIS measurements were carried out via a "Cary 60 UV-VIS" by "Agilent Technologies". For evaluation the software "spekwin 32" was used.

5.4   EPR Spectroscopy

The Cw-EPR measurements were carried out via a "Bruker EMX X-band EPR spectrometer" with 100 kHz field modulation. 2 mW microwave power and 0.1 mT modulation amplitude were used as conditions. The spectra were analyzed using WinSim and the g-factors determined by using DPPH solution (g= 2.0036) in THF as reference. [66]

5.5   ATR-FTIR

The ATR-FTIR measurements were conducted quickly in air with "ALPHA-P" by "Bruker" in total reflection mode.

5.6   Microwave

The Microwave Reactor "Monowave 300" by Anton Paar was used with 30 ml microwave vials.

5.7 Synthesis

5.7.1 Synthesis of Cl$_2$SnTPP
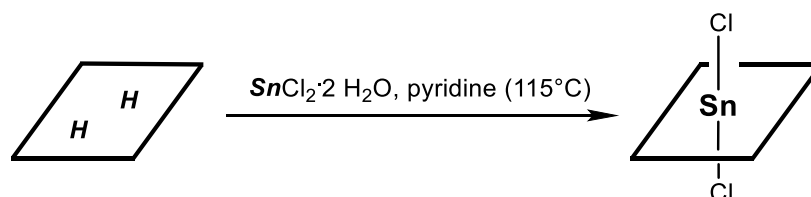
Scheme 10 Reaction of H$_2$TPP with SnCl$_2$*2H$_2$O yielding Cl$_2$SnTPP

The synthesis of Cl$_2$SnTPP was performed according to [15]. 2.02 g *meso*-Tetraphenyl porphyrin (TPPH$_2$) (3.3 mmol, 1.0 eq) and 2.352 g SnCl$_2$.2H$_2$0 (10.4 mmol, 3.1 eq) were added into a 1000 ml 1-neck round bottom flask, dissolved in 400 ml of commercially available pyridine and refluxed for 3.5 hours. A color change of the solution of purple to greenish/red can be observed. After cooling down the solution with an ice bath 400 ml deionized H$_2$O were added to the crude product and stirred for 15 min. The precipitate was then separated by centrifugation at 2000 rpm and 5 min. After washing with 80 ml deionized H$_2$O, 80 ml 1M HCl and 80 ml deionized H$_2$O the precipitate was dissolved in 180 ml HCCl$_3$, filtered and the solvent removed using a water trap. The excess SnCl$_2$*2H$_2$O was removed via sublimation and the excess water removed with 80 ml toluene via a water trap. This resulted in an amorphous purple solid (68% yield). ^{1}H-NMR (C$_6$D$_6$): 9.04 (s, ^{4}J$_{SnH}$ 14.62 Hz, 8H), 7.87 (d, ^{3}J$_{HH}$ 7.02 Hz, 8H), 7.46-7.33 (m, 12H); ^{119}Sn(C$_6$D$_6$): -588,6 (s); UV/VIS (THF; λ(nm)/rel Int): 405/0.12; 426/2.01; 522/0.01; 562/0.06; 601/0.04;

5.7.2 Synthesis of Cl₂GeTPP
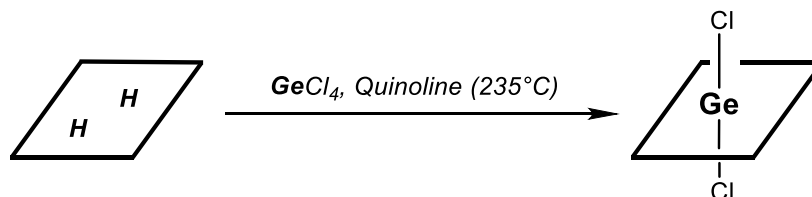
Scheme 11 Reaction of H₂TPP with GeCl₄ yielding Cl₂GeTPP

The synthesis of Cl$_2$GeTPP was performed according to [15]. 0.25 g TPPH$_2$ (0.41 mmol, 1 eq), 3 ml quinoline and 0.7 ml GeCl$_4$ (6.13 mmol, 14 eq) were added under inert atmosphere to a 20 ml microwave suitable flask and heated up to 235 °C (7.9 bar) for 1h using a microwave heater. After cooling to RT, the flask was centrifuged at 2000 rpm for 1h. The precipitate was isolated and transferred to a Schlenk vessel with 30 ml toluene. To remove the remaining quinoline, 3x 30 ml toluene was distilled off to drag the quinoline out. The purple solid was dried under vacuum at 60 °C giving a yield of 45%. ^{1}H-NMR (C$_6$D$_6$): 9.00 (s, 8H), 7.86 (d, ^{3}J$_{HH}$ 7.72 Hz, 8H), 7.33 (m, 12H); UV/VIS (THF; λ(nm)/rel Int): 407/0.18; 428/2.67; 519/0.02; 651/0.10; 600/0.06;

5.7.3 Attempted Synthesis of H₂SnTPP using NaH
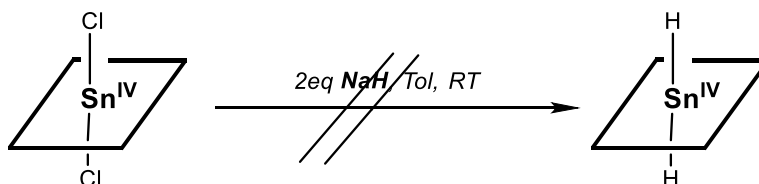
Scheme 12 Reaction of Cl₂SnTPP with NaH

51.2 mg (0.064 mmol, 1 eq) Cl$_2$SnTPP were placed into a 50 ml Schlenk under inert atmosphere and dissolved in 30 ml dry toluene. In a 10 ml Schlenk 5 mg NaH (0.208 mmol, 3.25 eq) were dissolved in 1 ml dry THF. At room temperature the NaH solution was added dropwise via syringe to the Cl$_2$SnTPP solution. No color change occurred. After stirring for 4h at RT no reaction had occurred. Thereon the solution was stirred under reflux heating for 4h. 7 ml of the solution were withdrawn and the solvent removed under vacuum, the purple powder was then dissolved in 0.5 ml C$_6$D$_6$ for NMR investigations. These showed a slight hydrolysis to (OH)$_2$SnTPP as well as

other byproducts yielding signals at: ^{1}H-NMR (C_6D_6): 9.08(s, 4 H), 9.04 (s, 8H), 8.78 (d, 3.46 Hz, 3H), 8.66 (brs, 19H), 8.32 (d, 8.21 Hz, 4H), 7.76 (m, 7 H), 7.43 (m, 23 H), 6.76 (m, 6H), -7.14 (s, 2H);

5.7.4 Attempted Synthesis of H₂SnTPP using BH₃
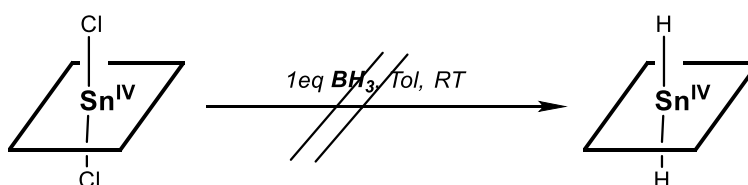
Scheme 13 Reaction of Cl₂SnTPP with BH₃

35.4 mg (0.044 mmol, 1 eq) Cl₂SnTPP were transferred into a 50 ml Schlenk under inert gas atmosphere and 10 ml dry toluene were added. After cooling to − 40 °C 0.045 ml (0.045 mmol, 1 eq) BH₃ solution (1M in THF) was added drop wise via syringe. After stirring for 7 days at RT no reaction occurred, leaving unreacted Cl₂SnTPP. ^{1}H-NMR (C_6D_6): 9.04 (s, 8H), 7.87 (d, $^3J_{HH}$ 6,7 Hz, 8H), 7.46-7.33 (m, 12H);

5.7.5 Attempted Synthesis of H₂SnTPP using DIBAL at RT

Scheme 14 Reaction of Reaction of Cl₂SnTPP with DIBAL yielding potentially *i*-BuAlTPP

53.2 mg (0.066 mmol, 1eq) Cl₂SnTPP were placed into a 50 ml Schlenk under inert gas atmosphere and dissolved in 30 ml dry toluene. Under stirring at RT 0.146 ml (0.146 mmol, 2.2 eq) DIBAL (1M in toluene) were added dropwise via syringe. A color change from purple to red/brown could be observed. 7 ml of the solution were withdrawn for NMR analysis, the solvent removed under vacuum and dissolved in 0.5 ml C₆D₆. The ^{1}H-NMR analysis showed 4 different porphyrin species (determined by the β-hydrogen atoms with a ratio of 0.52 : 0.47 : 2.01 : 10.00), among which

i-BuAlTPP is of highest intensity. ^{1}H-NMR (C$_6$D$_6$): 9.16(s), 9.14(s), 9.10(s), **9.09** (s), 8.11 (d, $^3J_{HH}$ 7.00 Hz), **7.99** (d, $^3J_{HH}$ 6.73 Hz), 7.87 (brs), 7.53- 7.34 (m), -1.03 (m), **-1.53** (d, 6.56 Hz), -2.10- (-2.33) (m), **-2.48** (hept), **-5.72** (d, $^3J_{HH}$ 6.61 Hz); UV/VIS (Toluene; λ(nm)/rel Int): 398/ 0.12, 418/0.50, 434/0.99, 490/0.02, 565/0.02, 606/0.02;

5.7.6 Attempted Synthesis of H$_2$SnTPP using DIBAL at -40 °C/ Synthesis of SnTPP
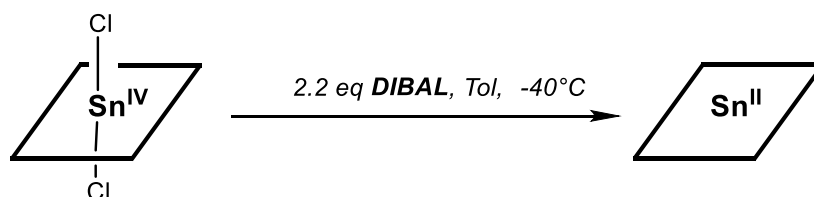
Scheme 15 Reaction of Cl$_2$SnTPP with DIBAL at -40 °C yielding SnTPP

The Synthesis was performed according to chapter 5.7.5 with exception of the reaction temperature. Upon adding the DIBAL solution the Cl$_2$SnTPP solution was cooled to -40 °C and stirred at this temperature for 15 min. The ^{1}H-NMR analysis showed 2 different porphyrin species (determined by the β-hydrogen atoms with a ratio of 0.76 : 10). ^{1}H-NMR (C$_6$D$_6$):): 9.10 (s), **9.08** (s), **8.12** (brs), 7.66 (brs), **7.56 -7.42** (m), -0.08 (m), -1.54 (d, 6.32 Hz), -1.93 (brs), -2.80 (brs), -3.59(brs);

The same reaction was performed at 0 °C. ^{1}H-NMR (C$_6$D$_6$): 9.13 (s), 9.10 (s), **9.08** (s), **8.12** (brs), 7.71 (brs), **7.51 -7.42** (m), -0.06 (m), -1.54 (d, 6.55 Hz), -1.77 (brs), -2.65 (brs);

5.7.7 Attempted Synthesis of H$_2$SnTPP using LiAlH$_4$/ Synthesis of SnTPP
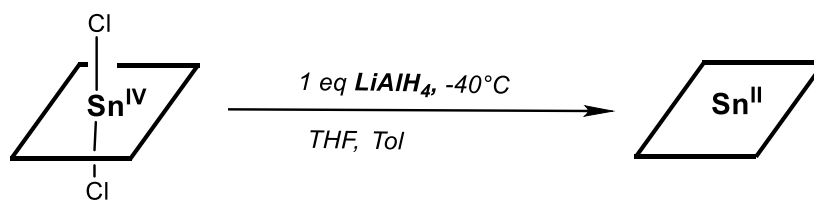
Scheme 16 Reaction of Cl$_2$SnTPP with LiAlH$_4$ at -40 °C yielding SnTPP

49.8 mg (0.062 mmol, 1 eq) Cl_2SnTPP were placed into a 50 ml Schlenk under inert gas atmosphere and dissolved in 30 ml dry toluene. 2.1 mg (0.055 mmol, 0.9 eq) $LiAlH_4$ were suspended in 2 ml dry THF. After cooling to -40 °C the $LiAlH_4$ suspension was added dropwise to the Cl_2SnTPP. An immediate color change from purple over red to green was detected. After 15 min the solvent was removed under vacuum. ^{1}H-NMR (C_6D_6): 9.08 (s, 8H), 8.12 (brs, 8H), 7.45 (m, 12H); UV/VIS (THF; λ(nm)/rel Int): 398/ 1.00, 464/0.31, 490/0.52, 700/0.07;

5.7.8 VT-NMR of Attempted Synthesis of H₂SnTPP using LiAlH₄/ Synthesis of SnTPP

For the VT-NMR study the reaction was performed according to 5.7.7 with THF-d_8 as solvent. After adding the $LiAlH_4$ suspension, 0.5 ml of the reaction mixture were transferred under inert gas atmosphere into an NMR Tube and sealed with parafilm. NMR and UV/VIS data are listed in Table 1 and Table 2.

5.7.9 Attempted Synthesis of H₂SnTPP using K[BEt₃]H/ Synthesis of SnTPP
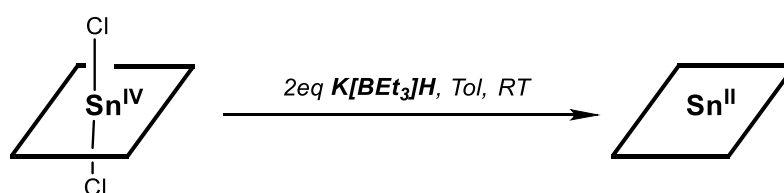
Scheme 17 Reaction of Cl_2SnTPP with K[BEt₃]H yielding SnTPP

22.8 mg (0.028 mmol, 1eq) Cl_2SnTPP were placed into a 20 ml Schlenk under inert gas atmosphere and dissolved in 8 ml dry toluene. After cooling the solution with an ice bath 0.08 ml K[Bet₃]H as a 1M solution in THF (0.08 mmol, 2.9 eq) were added dropwise using a syringe. A color change from purple to red to green/red in a matter of seconds could be observed. After stirring for 10 min the solvent was removed under vacuum. For NMR Analysis the product was solved in 0.5 ml C_6D_6. ^{1}H-NMR (C_6D_6): 9.08 (s, 8H), 8.12 (brs, 8H), 7.45 (m, 12H); UV/VIS (C_6D_6; λ(nm)/rel Int): 399/1.16, 426/1.39, 440/0.71, 490/0.51, 564/0.09;

5.7.10 Synthesis of Et₂SnTPP
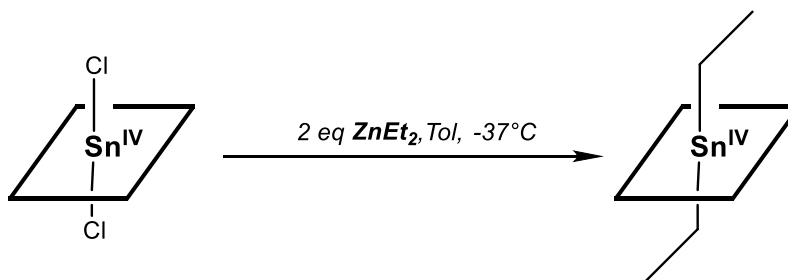
Scheme 18 Reaction of Cl₂SnTPP with 2 eq ZnEt₂ at -40 °C yielding Et₂SnTPP

The Synthesis of Et$_2$SnTPP was performed according to [67].

23.8 mg (0.029 mmol, 1 eq) Cl$_2$SnTPP were added to 20 ml toluene in a 50 ml Schlenk under inert gas atmosphere. After cooling to -37 °C 0.03 ml (0.03 mmol, 1 eq) ZnEt$_2$ (1 M in hexane) were added dropwise via syringe. The solution was stored in the freezer at -20 °C over night. The next day a purple/green color was detected and the solvent removed under vacuum. ^{1}H- NMR analysis showed both the product as well as the educt with a ratio of 1 : 0.54 (as determined by the integrals of the β-H atoms). ^{1}H-NMR (C$_6$D$_6$): 9.04 (s, 8H), 9.00 (s, 8H), 8.16 (d, $^3J_{HH}$ 7.24 Hz, 8H), 7.84 (d, $^3J_{HH}$ 7.57 Hz, 8H), 7.44 (m, 24H), -3.61 (t, $^4J_{SnH}$ 10.37 Hz, 6H), -6.28 (q, $^2J_{SnH}$ 53.63 Hz, 4H); UV/VIS (C$_6$D$_6$; λ(nm)/rel Int): 364/0.06, 407/0.06, 429/0.79, 554/0.41, 564/0.02, 622/0.03, 662/0.03;

5.7.11 Synthesis of (*i*-Bu)₂SnTPP
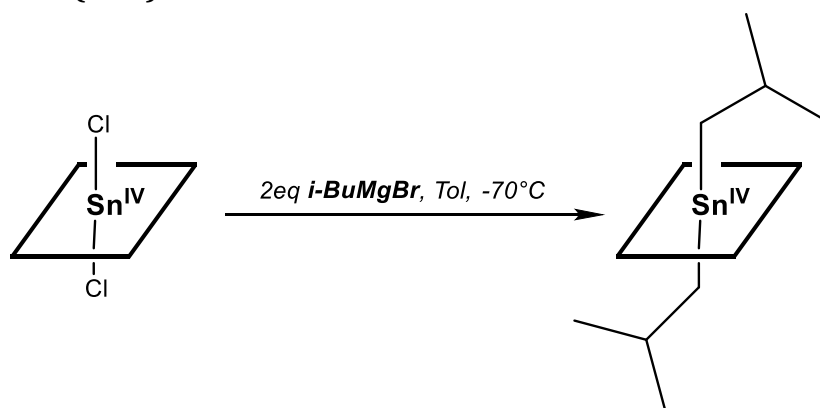
Scheme 19 Reaction of Cl₂SnTPP with 2 eq *i*-BuMgBr at -40 °C yielding (*i*-Bu)₂SnTPP

The Synthesis was performed similar to [60].

18.5 mg (0.023 mmol, 1 eq) Cl_2SnTPP were dissolved in 10 ml dry toluene. After cooling the solution to – 70 °C 0.03 ml (0.06 mmol, 2.6 eq) *i*-BuMgBr solution (2M in diethylether) was added dropwise using a syringe. The solution was then stirred for 1h at – 70 °C. After reaching RT the solvent was removed under vacuum. ^{1}H-NMR showed the contamination of the product with 2 other unidentified porphyrin species (ratio 1: 0.18 : 0.17, as determined by the integrals of the β-H atoms). ^{1}H- NMR (C_6D_6): 9.00 (s, 8H), 8.22 (d, $^3J_{HH}$ 7.24 Hz, 8H), 7.03 (m, 19H), -1.95 (d, 6.47 Hz, 12 H), -3.96 (hept, 2H), -6.49 (d, $^2J_{HH}$ 6.10 Hz, $^4J_{SnH}$ 53.58 Hz, 4H); UV/VIS (C_6D_6; λ(nm)/rel Int): 376/0.19, 432/0.25, 456/0.99, 568/0.007, 617/0.02, 667/0.09;

5.7.12 Synthesis of H₂GeTPP
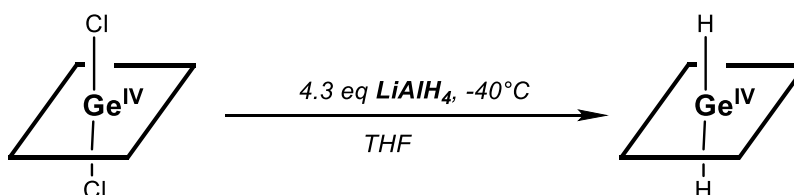
Scheme 20 Reaction of Cl₂GeTPP with 1eq LiAlH₄ yielding H₂GeTPP

5.9 mg (7.8 μmol, 1eq) Cl_2GeTPP were transferred into a 20 ml Schlenk under inert gas atmosphere and 4 ml dry THF added. After cooling to – 40° C 0.32 ml (16.8 μmol, 4.3 eq) of a $LiAlH_4$ suspension (0.0522 M in THF) was added. Immediate color change from purple to green occurred. The solution was filtered through silica. ^{1}H-NMR (C_6D_6): 9.07 (s, 8H), 8.07 (d, $^3J_{HH}$ 7.01 Hz, 8H), 7.43 (m, 12H), -3.09 (s, 2H); UV/VIS (C_6D_6; λ(nm)/rel Int): 347/0.05, 417/0.30, 454/0.93, 496/0.01, 613/0.01, 659/0.08;

5.7.13 VT-NMR of H₂GeTPP

The reaction was performed according to 5.7.12 with THF-d_8 as solvent, 0.5 ml transferred into an NMR tube and sealed with parafilm. The NMR data is listed in Table 7.

5.7.14 Synthesis of Cl₂SiTPP
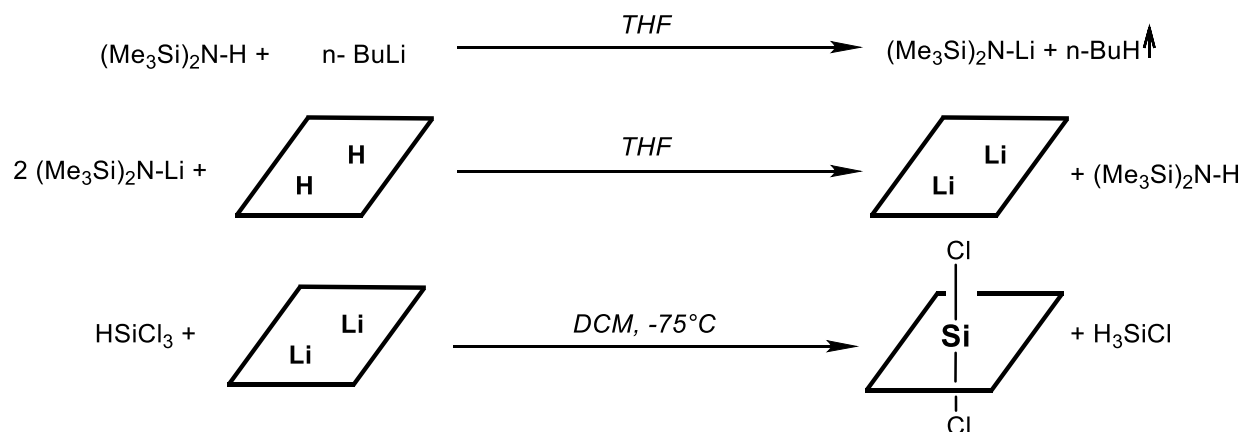
Scheme 21 Reaction yielding Cl₂SiTPP

The synthesis of Cl$_2$SiTPP was performed by [18] according to [68] but is mentioned for the sake of completeness.

In a 50 ml Schlenk 30 ml dry THF and 0.39 ml (1.9 mmol, 2.3 eq) HMDS (Hexamethyldisilazane) were added and cooled to 10 °C. 0.73 ml (1.83 mmol, 2.2 eq) n-BuLi were added dropwise and the solution refluxed for 1h. In a two-neck flask 0.502 g (0.82 mmol, 1 eq) H$_2$TPP were dissolved in 20 ml dry THF. The LiN(SiMe$_3$)$_2$ solution was added subsequently via a syringe to the H$_2$TPP solution. A color change to blue occurred. The solution was refluxed for 4h and stirred overnight. The next day the reaction mixture was refluxed again for 1h. Then the solvent was removed under vacuum.

The precipitate was again dissolved in 20 ml DCM and cooled to – 75 °C. 0.13 ml (1.27 mmol, 1.6 eq) HSiCl$_3$ were added dropwise and the solution stirred at -75 °C for 2h. After warming to RT the reaction mixture was refluxed for 15 min. The solvent was removed under vacuum and dissolved in 35 ml DCM again. The white precipitate was filtered off and the solvent removed again under vacuum. The product was crystallized from 20 ml THF.

^{1}H-NMR (C$_6$D$_6$): 8.85 (s, 8H), 7.76 (d, [3]J$_{HH}$ 7.09 Hz, 8H), 7,29 (m, 12H); ^{29}Si-NMR (CDCl$_3$): -217.3; UV/VIS (C$_6$D$_6$; λ(nm)/rel Int): 414/0.08; 438/0.99; 569/0.03; 609/0.02;

5.7.15 Synthesis of H$_2$SiTPP
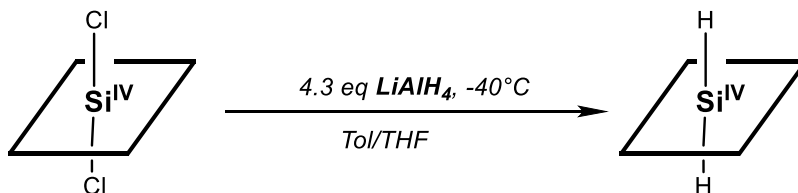
Scheme 22 Reaction of Cl$_2$SiTPP with 1eq LiAlH$_4$ yielding H$_2$SiTPP

7.5 mg (9.9 µmol, 1eq) Cl$_2$SiTPP were transferred into a 20 ml Schlenk under inert gas atmosphere and dissolved in 2 ml toluene. After cooling to – 40 °C 0.011 ml (42.9 µmol, 4.3 eq) of a LiAlH$_4$ suspension (0.0522 M in THF) was added. A color change from blue to green occurred in a matter of seconds. ^{1}H-NMR (C$_6$D$_6$): 8.99 (s, 8H), 7.93 (d, $^3J_{HH}$ 6.03 Hz, 8H), 7.38 (m, 12H), -4.36 (s, 2H); UV/VIS (C$_6$D$_6$; λ(nm)/rel Int): 419/0.11, 439/0.19, 462/0.99, 626/0.045, 673/0.12;

6 References

[1] F. Bryden, R. W. Boyle, Metalloporphyrins for Medical Imaging Applications, in: Insights from Imaging in Bioinorganic Chemistry, Elsevier, 2016 pp. 141–221.

[2] E. A. Berry, M. Guergova- Kuras, L. S. Huang, A. R. Crofts, Mechanism of Ubiquinol Oxidation by the bc_1 Complex: Role of the Iron Sulfur Protein and Its Mobility, Annu. Rev. Biochem. (2000) 1005–1075.

[3] G. E. Ficken, R.B. Johns, R.P. Linstead, Chlorophyll and Related Compounds. Part IV, J. Chem. Soc. (1956) 2272–2280.

[4] M. Momenteau, C. A. Reed, Synthetic Heme-Dioxygen Complexes, Chem. Rev. 1994 659–698.

[5] J.Z. M. Nencki, Untersuchungen über den Blutfarbstoff, Hoppe-Seyler´s Zeitschrift für physiologische Chemie 30 (1900) 384–435.

[6] B. W. Pogue, B. Ortel, N. Chen, R. W. Redmond, T. Hasan, A Photobiological and Photophysical-based Study of Phototoxity of Two Chlorins, Cancer Res (2001) 717–724.

[7] J. Zhuo (Ed.), Antimicrobial Textiles, Elsevier, 2016.

[8] W. Kim, T. Tachikawa, T. Majima, C. Li, H.- J. Kim, Hee-Joon, W. Choi, Tin-porphyrin sensitized TiO_2 for the production of H2 under visible light, Energy Environ. Sci. 3 (2010) 1789.

[9] J. Hatano, N. Obata, S. Yamaguchi, T. Yasuda, Y. Matsuo, Soluble porphyrin donors for small molecule bulk heterojunction solar cells, J. Mater. Chem. 22 (2012) 19258.

[10] H. Qin, L. Li, G. Lisheng, S. Fangqing, P. Shijian, C. Junbiao, P. Yong, Xiaobin, Solution-processed bulk heterojunction solar cells based on a porphyrin small molecule with 7% power conversion efficiency, Energy Environ. Sci. 7 (2014) 1397–1401.

[11] S. Mathew, A. Yella, P. Gao, R. Humphry-Baker, B. F. E. Curchod, N. Ashari-Astani, I. Tavernelli, U. Rothlisberger, Md K. Nazeeruddin, M. Grätzel, Dye-sensitized solar cells with 13% efficiency achieved through the molecular engineering of porphyrin sensitizers, Nature chemistry 6 (2014) 242–247.

[12] CN105694526 2016.

[13] M. E. Thompson, US2017092883A1 (2016) 1–61.

[14] S. R. Forrest, EP 2 470 543 B1 (2010) 1–121.

[15] S. Stadlbauer, R. Fischer, M. Flock, P. Zach, S. Borisov, A. Torvisco, F. Uhlig, Structure and spectroscopic properties of porphyrinato group 14 derivatives: Part I – Phenylacetylido ligands, Zeitschrift für Naturforschung B 72 (2017) 801–811.

[16] S. Stadlbauer, D. Grössl, R. Fischer, N. Demitri, F. Uhlig, Redistribution reaction on six- fold coordinated Sn(IV) atom and access to axially un symmetric substituted Sn(IV) porphyrins, Inorg. Chem., submitted (2020).

[17] D. P. Arnold, J. Blok, The coordination chemistry of tin porphyrin complexes, Coordination Chemistry Reviews 248 (2004) 299–319.

[18] S. Stadlbauer, Organometallic group 14 metal dyes in thin film organic solar cells, PhD Thesis, TU Graz, 2019.

[19] P. J. Brothers, Organoelement Chemistry of Main-Group Porphyrin Complexes pp. 289–342.

[20] J.- Y. Zheng, T.A. J. Konishi, A Photoresponsive Silicon Radical within a Porphyrin π-Cloud: Photolysis of Organo- and Nitroxysilicon Porphyrins with Visible Light, J. Am. Chem. Soc. (1998) 9838–9843.

[21] Maskasky, Joe E., Kenney, Malcolm E., Macrocyclic nuclear magnetic resonance shift reagents, J. Am. Chem. Soc. 95 (1973) 1443–1448.

[22] C. Cloutour, D. Lafargue, J. C. Pommier, Monophotooxydation selective de dialkylgermylet -stannylporphyrines, Journal of Organometallic Chemistry 190 (1980) 35–42.

[23] P. J. Brothers, Recent developments in the coordination chemistry of porphyrin complexes containing non-metallic and semi-metallic elements, J. Porphyrins Phthalocyanines 06 (2002) 259–267.

[24] K. M. Kadish, K. M. Smith, R. Guilard, Handbook of Porphyrin Science (Volume 16), World Scientific Publishing Company, 2012.

[25] J. Chen, L. K. Woo, Syntheses and Characterizations of Alkyl- and Amidotin Porphyrin Complexes: Molecular Structure of trans-Bis(phenylacetylido)(meso-tetra-p-tolylporphyrinato)tin(IV), Inorg. Chem. (1998) 3269–3275.

[26] D. Y. Dawson, J. C. Sangalang, J. Arnold, Stereochemical Control in Metalloporphyrin Chemistry: Synthesis and Characterization of cis- and trans-Sn(porphyrin)Ph$_2$, J. Am. Chem. Soc. (1996) 6082–6083.

[27] A. G. Davies, Recent advances in the chemistry of the organotin hydrides, j. chem. res. (s) (2006) 141–148.

[28] A. G. Davies, Organotin chemistry, John Wiley & Sons, Mississauga, Ont., 2004.

[29] J. Turek, Z. Padělková, Z. Černošek, M. Erben, A. Lyčka, M. Nechaev, I. Císařová, A. Růžička, C,N-chelated hexaorganodistannanes, and triorganotin(IV) hydrides and cyclopentadienides, Journal of Organometallic Chemistry 694 (2009) 3000–3007.

[30] Z.R. S. Patai, The chemistry of organic germanium, tin, and lead compounds, 1995.

[31] Md. M. M. Khan, S. Ghosh, G. Hogarth, D. Tocher, M. G. Richmond, S. E. Kabir, H. W. Roesky, Mixed main group transition metal clusters: Reactions of [Ru$_3$(CO)$_{10}$ (μ-dppm)] with Ph$_3$SnH, Journal of Organometallic Chemistry 840 (2017) 47–55.

[32] U. Schubert, S. Gilbert, S. Mock, Transition-Metal Silyl Complexes, 43[1] Preparation and Fluxionality of the Complexes FeH$_3$(PPh$_2$R')$_3$ER$_3$ (E = Si, Sn; R' = Et,nBu), Chem. Ber. 125 (1992) 835–837.

[33] F. Bitto, K. Kraushaar, U. Böhme, E. Brendler, J. Wagler, E. Kroke, Chlorosilanes and 3,5-Dimethylpyrazole: Multinuclear Complexes, Acetonitrile Insertion and ^{29}Si-NMR Chemical-Shift Anisotropy Studies, Eur. J. Inorg. Chem. 2013 (2013) 2954–2962.

[34] I. Kalikhman, B. Gostevskii, V. Kingston, S. Krivonos, D. Stalke, B. Walfort, T. Kottke, N. Kocher, D. Kost, Spin Coupling through the N→Si Dative Bond in Penta- and Hexacoordinate Hydrido- and Fluorosilicon Complexes; Coupling through a Rapidly Dissociating–Recombining N→Si Bond, Organometallics 23 (2004) 4828–4835.

[35] W. Levason, D. Pugh, G. Reid, Phosphine and diphosphine complexes of silicon(IV) halides, Inorg. Chem. 52 (2013) 5185–5193.

[36] G. W. Fester, J. Eckstein, D. Gerlach, J. Wagler, E. Brendler, E. Kroke, Reactions of hydridochlorosilanes with 2,2'-bipyridine and 1,10-phenanthroline: complexation versus dismutation and metal-catalyst-free 1,4-hydrosilylation, Inorg. Chem. 49 (2010) 2667–2673.

[37] G. W. Fester, J. Wagler, E. Brendler, E. Kroke, Stable Trichlorosilane-Pyridine Adducts, Eur. J. Inorg. Chem. 2008 (2008) 5020–5023.

[38] S. Stadlbauer, Potentielle Donormoleküle für Bulk-Hetero-Junction Photovoltaikzellen, Master Thesis, TU Graz, 2015.

[39] E. D. Becker, R. B. Bradley, Effects of "Ring Currents'' on the NMR Spectra of Porphyrins, The Journal of Chemical Physics 31 (1959) 1413–1414.

[40] S. Pelloni, A. Ligabue, P. Lazzeretti, Ring-current models from the differential Biot-Savart law, Organic letters 6 (2004) 4451–4454.

[41] D.P. Arnold, Spectroscopic cis-influences in octahedral tin(IV) meso-tetraphenylporphyrin complexes, Polyhedron 5 (1986) 1957–1963.

[42] A. L. Balch, C. R. Cornman, M. M. Olmstead, Formation and structure of alkyl peroxide complexes of germanium(IV) porphyrins from direct reactions with alkyl hydroperoxides and by photolysis of alkylgermanium(IV) porphyrins in the presence of dioxygen, J. Am. Chem. Soc. (1990) 2963–2969.

[43] T. R. Janson, A. R. Kane, J. F. Sullivan, K. Knox, M. E. Kenney, Ring-current effect of the phthalocyanine ring, J. Am. Chem. Soc. (1969) 5210–5214.

[44] V. N. Nemykin, R. G. Hadt, Interpretation of the UV-vis spectra of the meso(ferrocenyl)-containing porphyrins using a TDDFT approach: is Gouterman's classic four-orbital model still in play?, The journal of physical chemistry. A 114 (2010) 12062–12066.

[45] M. Gouterman, Spectra of porphyrins, Journal of Molecular Spectroscopy 6 (1961) 138–163.

[46] J. M. Barbe, C. Ratti, P. Richard, C. Lecomte, R. Gerardin, R. Guilard, Tin(II) porphyrins: synthesis and spectroscopic properties of a series of divalent tin porphyrins. X-ray crystal

structure of (2,3,7,8,12,13,17,18-octaethylprophinato)tin(II), Inorg.Chem. (1990) 4126–4130.

[47] D. W. H. Rankin, N. W. Mitzel, C. A. Morrison, Structural methods in molecular inorganic chemistry, Wiley, Chichester, 2013.

[48] The Porphyrins, Elsevier, 1979.

[49] J. FAJER, M. S. DAVIS, Electron Spin Resonance of Porphyrin π Cations and Anions, in: The Porphyrins, Elsevier, 1979 pp. 197–256.

[50] J. A. Cissell, T. P. Vaid, G. P. A. Yap, Reversible oxidation state change in germanium(tetraphenylporphyrin) induced by a dative ligand: aromatic Ge^{II}(TPP) and antiaromatic Ge^{IV}(TPP)(pyridine)$_2$, Journal of the American Chemical Society 129 (2007) 7841–7847.

[51] G. B. Maiya, J. M. Barbe, and K. M. Kadish, Photoreactivity of .sigma.-bonded metalloporphyrins. 2. Germanium porphyrin complexes with sigma-bonded alkyl, aryl, or ferrocenyl groups. Intramolecular quenching of porphyrin excited triplet states by linked ferrocene, Inorg. Chem. (1989) 2524–2527.

[52] E. De Boer, H. Van Willigen, Chapter 3 Nuclear magnetic resonance of paramagnetic systems, Progress in Nuclear Magnetic Resonance Spectroscopy 2 (1967) 111–161.

[53] H. Günther, NMR spectroscopy. Basic principles, concepts, and applications in chemistry, Wiley-VCH, Weinheim, Germny, 2013.

[54] F. H. Allen, I. J. Bruno, Bond lengths in organic and metal-organic compounds revisited: X-H bond lengths from neutron diffraction data, Acta crystallographica. Section B, Structural science 66 (2010) 380–386.

[55] G. Du, A. Ellern, K. L. Woo, Reaction of tin porphyrins with vicinal diols, Inorg. Chem. 43 (2004) 2379–2386.

[56] Z. Ou, E. Zhongping, Z. Wenbo, T. Weihua, S. Pall, J. Paul, M. Crossley, J. Maxwell, K. Kadish, Effect of axial ligands and macrocyclic structure on redox potentials and electron-transfer mechanisms of SnIV porphyrins, Inorg. Chem. 46 (2007) 10840–10849.

[57] K. M. Kadish, Q. Y. Xu, G. Maiya, J. M. Barbe, R. Guilard, Effect of axially bound anions on the electroreduction of tin(IV) porphyrins in tetrahydrofuran, J. Chem. Soc., Dalton Trans. (1989) 1531.

[58] S. S. Eaton, R. Gareth, Phenyl ring rotation in metal complexes of tetraphenylporphyrin derivatives, J. Chem. Soc. (1974) 576.

[59] G. A. Webb, D. B. Davies, Nuclear magnetic resonance. A review of the literature published between June 1979 and May 1980, Royal Society of Chemistry, London, 1981.

[60] C. Cloutour, C. Debaig-Valade, C. Gacherieu, J.-C. Pommier, Etude comparative de l'alkylation des tetraphenylporphyrines de l'etain et de leurs formes reduites par les reactifs de grignard, Journal of Organometallic Chemistry 269 (1984) 239–247.

[61]   R. Guilard, A. Zrineh, A. Tabard, A. Endo, B. C. Han, C. Lecomte, M. Souhassou, A. Habbou, M. Ferhat and K. M. Kadish, Synthesis and spectroscopic and electrochemical characterization of ionic and sigma.-bonded aluminum(III) porphyrins. Crystal structure of methyl(2,3,7,8,12,13,17,18-octaethylporphinato)aluminum(III), (OEP)Al(CH$_3$), Inorg.Chem. (1990) 4476–4482.

[62]   S. - J. Lin, Y.-J. Chen, J.-H. Chen, F.-L. Liao, S.- L. Wang, S.- S. Wang, Crystal structures of chloro(meso-tetraphenylporphyrinato)germanium(IV), Ge(tpp)Cl$_2$, and dihydroxo(meso-tetraphenylporphyrinato)germanium(IV), Ge(tpp)(OH)$_2$, and two-stage hydrolysis of its homologue dimethoxo(meso-tetraphenylporphyrinato)germanium(IV), Ge(tpp)(OMe)$_2$, Polyhedron 16 (1997) 2843–2850.

[63]   M. Traxler, Synthesis and Application of Organogermanium Compounds: From Small Metallorganic Precursors towards Functional Nano Sized Particles, Master Thesis, TU Graz, 2019.

[64]   K. Kadish, E. van Caemelbecke, Electrochemistry of Metalloporphyrins in Nonaqueous Media, in: A. J. Bard (Ed.) Encyclopedia of Electrochemistry, Wiley-VCH Verlag GmbH & Co. KGaA, Weinheim, Germany, 2007 p. 435.

[65]   J. Y. Zheng, K. Konishi, T. Aida, Dioxygen Insertion into the Axial Si-C Bonds of Organosilicon Porphyrins, Chem. Lett. 27 (1998) 453–454.

[66]   D. R. Duling, Simulation of multiple isotropic spin-trap EPR spectra, Journal of magnetic resonance. Series B 104 (1994) 105–110.

[67]   J. Chen, K. L. Woo, Syntheses and Characterizations of Alkyl- and Amidotin Porphyrin Complexes: Molecular Structure of trans -Bis(phenylacetylido)(meso -tetra- p - tolylporphyrinato)tin(IV), Inorg. Chem. 37 (1998) 3269–3275.

[68]   K. M. Kane, C. R. Lorenz, D. M. Heilman, F. R. Lemke, Substituent Effects on the Spectroscopic Properties and Reactivity of Hexacoordinate Silicon(IV) Porphyrin Complexes, Inorg. Chem. 37 (1998) 669–673.

7 Appendix

7.1 Table of Figures

7.2 Table of Schemes

7.3 Table of Tables

7.4   Table of Equations

7.5   NMR

7.5.1 ^{1}H-NMR of Cl_2SnTPP in C_6D_6

7.5.2 ^{1}H-NMR of Cl$_2$GeTPP in C$_6$D$_6$
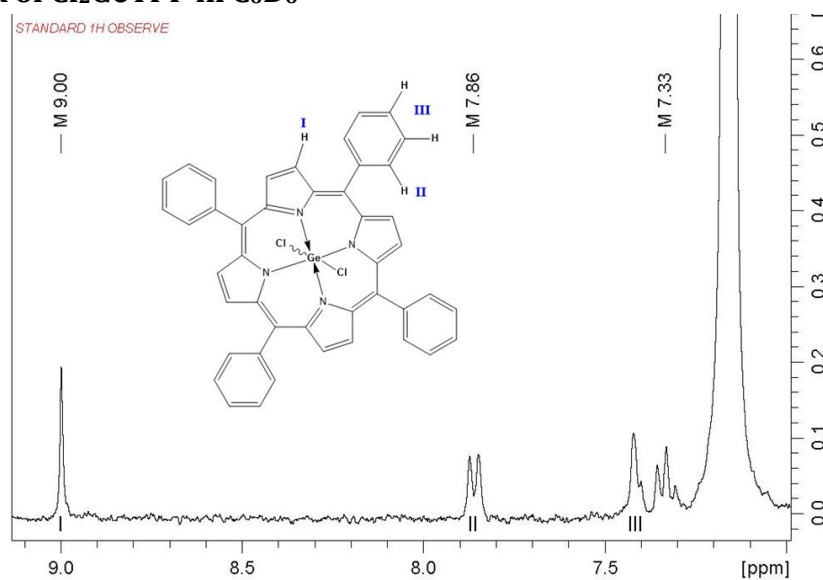
7.5.3 ^{1}H-NMR of Et$_2$SnTPP with side products in C$_6$D$_6$